NASA/TP–20240002920

Airfoil Table Modification for Improved Calculation of Ingenuity Rotor Performance

Joshua Bowman, Michelle Dominguez, Wayne Johnson, Witold J. F. Koning,
Gianmarco Sahragard-Monfared, Natasha Schatzman, Stephen Wright
Moffett Field, California

March 2024

NASA STI Program ... in Profile

Since its founding, NASA has been dedicated to the advancement of aeronautics and space science. The NASA scientific and technical information (STI) program plays a key part in helping NASA maintain this important role.

The NASA STI program operates under the auspices of the Agency Chief Information Officer. It collects, organizes, provides for archiving, and disseminates NASA's STI. The NASA STI program provides access to the NTRS Registered and its public interface, the NASA Technical Reports Server, thus providing one of the largest collections of aeronautical and space science STI in the world. Results are published in both non-NASA channels and by NASA in the NASA STI Report Series, which includes the following report types:

- TECHNICAL PUBLICATION. Reports of completed research or a major significant phase of research that present the results of NASA Programs and include extensive data or theoretical analysis. Includes compilations of significant scientific and technical data and information deemed to be of continuing reference value. NASA counter-part of peer-reviewed formal professional papers but has less stringent limitations on manuscript length and extent of graphic presentations.

- TECHNICAL MEMORANDUM. Scientific and technical findings that are preliminary or of specialized interest, e.g., quick release reports, working papers, and bibliographies that contain minimal annotation. Does not contain extensive analysis.

- CONTRACTOR REPORT. Scientific and technical findings by NASA-sponsored contractors and grantees.

- CONFERENCE PUBLICATION. Collected papers from scientific and technical conferences, symposia, seminars, or other meetings sponsored or co-sponsored by NASA.

- SPECIAL PUBLICATION. Scientific, technical, or historical information from NASA programs, projects, and missions, often concerned with subjects having substantial public interest.

- TECHNICAL TRANSLATION. English-language translations of foreign scientific and technical material pertinent to NASA's mission.

Specialized services also include organizing and publishing research results, distributing specialized research announcements and feeds, providing information desk and personal search support, and enabling data exchange services.

For more information about the NASA STI program, see the following:

- Access the NASA STI program home page at http://www.sti.nasa.gov

- E-mail your question to help@sti.nasa.gov

- Write to:
  NASA STI Information Desk
  Mail Stop 148
  NASA Langley Research Center
  Hampton, VA 23681-2199

NASA/TP–20240002920

Airfoil Table Modification for Improved Calculation of Ingenuity Rotor Performance

Joshua Bowman, Michelle Dominguez, Wayne Johnson, Witold J. F. Koning, Gianmarco Sahragard-Monfared, Natasha Schatzman, Stephen Wright
Ames Research Center
Moffett Field, California

National Aeronautics and
Space Administration

Ames Research Center
Moffett Field, CA 94035-1000

March 2024

This report is available in electronic form at

http://ntrs.nasa.gov

Nomenclature

α	=	Angle of Attack
α_{ref}	=	Reference Angle of Attack for Airfoil Table Modifications
c	=	Airfoil Section Chord
c_d	=	Airfoil Section Drag Coefficient
c_l	=	Airfoil Section Lift Coefficient
c_m	=	Airfoil Section Pitching Moment
C_P	=	Rotor Power Coefficient
C_T	=	Rotor Thrust Coefficient
FM	=	Figure of Merit
k	=	Airfoil Table Modification Multiplicative Factor
ρ	=	Atmospheric Density in kg/m^3
σ	=	Rotor Solidity
t/c	=	Airfoil Thickness to Chord Ratio
x	=	Airfoil Table Modification Exponential Factor
x/c	=	Airfoil x Coordinate Normalized Relative to Chord
y/c	=	Airfoil y Coordinate Normalized Relative to Chord
y+	=	Dimensionless Wall Distance for Computational Fluid Dynamics

Abstract

To better characterize the behavior of the Ingenuity helicopter, multiple test campaigns were conducted. These tests included the Engineering Design Model 1 (EDM1) tests and the Transonic Rotor Test (TRT), both of which assessed Ingenuity rotor performance at various conditions. Using a comprehensive rotorcraft analysis tool, CAMRAD II, test setups of the two different Ingenuity test campaigns were simulated. The EDM1 test used coaxial test stand which focused on varying collective at various feasible Martian atmospheric densities and the TRT test used a single rotor test stand which focused on varying RPM to assess performance at different blade tip Mach numbers. Initial CAMRAD II analyses yielded performance results which differed significantly from experimental results. To reconcile the experimental results and the CAMRAD II analyses, modifications were made to the input airfoil decks for CAMRAD II. After several iterations of modifications, a specific method of modification was found that more accurately predicted experimental behavior at all tested densities for the coaxial rotor. This same modification was less successful for the single rotor test results. There are a number of differences between coaxial and single rotor aerodynamics and between the two test stands (hub and control system); also, there is a small influence of RPM (mainly tip Mach number) on dimensionless performance. These differences may be causing the coaxial rotor modifications not being successful for the single rotor.

Introduction

Due to the success of the Ingenuity rotorcraft on Mars, the use of two additional Ingenuity-style rotorcraft has been proposed for the purposes of Mars Sample Return [1].[1] To maintain heritage, the two Sample Return Helicopters (SRHs) will be of very similar design to Ingenuity, with the addition of a robotic arm, wheels, and an increased rotor size. To further validate the performance of Ingenuity, two test campaigns were launched using the Ingenuity rotor.

Engineering Design Model 1 (EDM1) tests for Ingenuity used a coaxial test stand to model the behavior of Ingenuity in multiple different Mars-like atmospheric densities in the JPL 25-Foot Space Simulator. The densities at which the EDM1 tests were conducted were 0.01, 0.0185, and 0.03 kg/m^3 with speeds ranging from 2430-2550 RPM. The EDM1 tests sought to determine the stall limit of the Ingenuity rotor by operating at high collective angles, up to 22.5 degrees [2].

The Transonic Rotor Test (TRT) was conducted using a single rotor at the 0.01 kg/m^3 density at multiple tip Mach number. The tip Mach numbers tested were 0.65, 0.7, 0.75, 0.8, and 0.85 (2740-3585 RPM) in the TRT tests. While the results from EDM1 were mainly focused on increasing collective at different atmospheric densities, the TRT tests were focused on determining the effects of varying the RPM at various collectives at a single atmospheric density of 0.01 kg/m^3 [2].

While this data provided valuable insight into the performance of Ingenuity and similar Mars coaxial rotorcraft, initial simulations in CAMRAD II, a comprehensive analysis tool for rotorcraft, yielded significantly different performance results, summarized in this report using the C_T/σ vs collective, FM vs C_T/σ, and C_P vs C_T curves. To better capture the experimental results using CAMRAD II, modifications to the airfoil tables used in CAMRAD II were proposed. The goal of these modifications was to provide improved predictive capabilities for future SRH testing by better capturing the behavior of the Ingenuity rotor tests. This technical memorandum focuses on the work in the modification of airfoil tables in an effort to better match CAMRAD II predictions with the experimental results of the EDM1 and TRT tests.

[1] The decision to implement Mars Sample Return will not be finalized until NASA's completion of the National Environmental Policy Act (NEPA) process. This document is being made available for information purposes only.

Rotor Performance Calculations

The rotor performance was calculated using CAMRAD II, a comprehensive analysis tool for rotorcraft [4,5]. CAMRAD II is an aeromechanics analysis of rotorcraft that incorporates multibody dynamics, nonlinear finite elements, and rotorcraft aerodynamics. The trim task finds the equilibrium solution for a steady state operating condition and produces the solution for performance, loads, and vibration. CAMRAD II has undergone extensive correlation of performance and loads measurements on rotorcraft, including coaxial rotors [6]. The CAMRAD II aerodynamic model for the rotor blade is based on lifting-line theory, using steady two-dimensional airfoil characteristics and a vortex wake model, plus models for unsteady flow (attached flow and dynamic stall) and yawed/swept flow. Effects of compressibility (Mach numbers) and viscosity (Reynolds number, stall, and drag) enter through airfoil table data: lift, drag, and moment coefficients of two-dimensional sections as function of angle of attack and Mach number, for the appropriate chord and atmosphere (density, temperature) so as to have correct Reynolds number variation with Mach number. The wake analysis calculates rotor nonuniform induced velocities, using free wake geometry. The vortex wake consists of rolled-up tip vortices and inboard vortex sheets, emanating from each blade. Second-order lifting-line theory provides accurate approximations of vortex-induced loading on the blades. Free wake geometry calculations give the self-induced distortion of the intertwined, interacting tip vortices, including the mutual interaction of the wake from the two coaxial rotors. The CAMRAD II blade structural model is based on nonlinear beam theory of rotating finite elements.

Airfoil Characteristics Calculation and Blade Geometry

The numerical approach for the airfoil deck generation for the as-manufactured Ingenuity rotor is described in Reference 7. Some elements are repeated here for the convenience of the reader.

Airfoil and rotor performance for all CFD simulations are obtained using structured grids and solved using the implicit, compressible Navier-Stokes solver OVERFLOW 2.3d [8,9]. Inviscid fluxes are computed using the HLLE++ flux schemes with a 5th-order WENOM upwind reconstruction approach for high spatial accuracy with low numerical dissipation [10]. Viscous fluxes are computed using second-order central differencing, as are grid metric terms. Time advance uses a second-order backward differencing scheme, with a dual time-stepping approach as described in References 11 and 12.

Earlier Ingenuity rotor models used turbulence and transition models in an effort to predict the sectional performance at compressible low Reynolds numbers [13,14]. A later study showed satisfactory correlation for Eppler 387 airfoil performance at low Reynolds numbers to experimental data when usinging laminar Unsteady Navier-Stokes (UNS) equations, meaning no turbulence model is implemented [15]. The study showed that mean behavior of unsteady Laminar Separation Bubbles (LSB) can be captured accurately using laminar UNS, and transition to turbulence was governed by a separated shear layer instability resulting in the shedding of large-scale coherent vortices, resulting in reattachment of the mean flow only [15]. Similar shear layer instabilities are observed in the sectional simulations for the Ingenuity rotor performance model, alluding to similar mechanisms at play and the relative importance of large-scale coherent motion, when compared to small-scale turbulence. A representative flow field for the r/R = 0.75 radial station is presented in Figure 1.

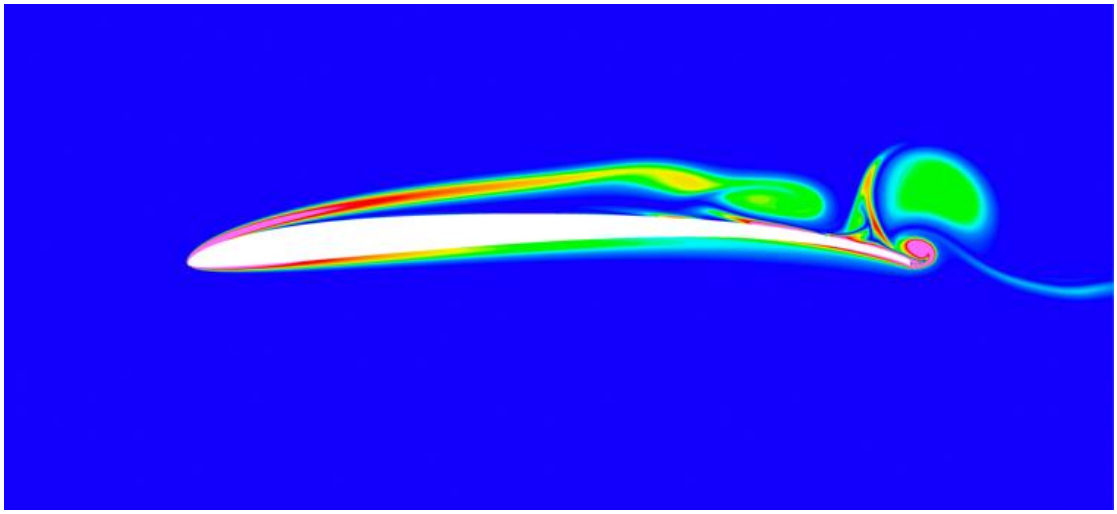

Figure 1: Ingenuity Airfoil r/R = 0.75, α = 6°, Instantaneous Vorticity Magnitude

The Ingenuity airfoil coordinates were interpolated to yield a high density set of coordinates [13]. In contrast to the geometry in Reference 14, airfoil geometry for all eight radial stations was not based on the original airfoil geometry design, but on the as-built geometry and extracted from the outer mold line (OML) Computer Aided Design (CAD) model. The main difference with the profiles used in Reference 14 is the constant thickness trailing edge on the actual Ingenuity rotor geometry of around 0.5 mm. Figure 2 through Figure 5 show the airfoil upper and lower surfaces at various radial stations.

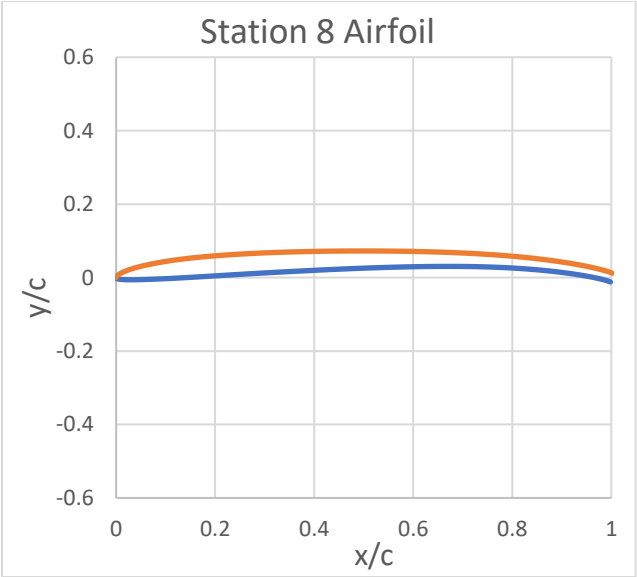

Figure 2: Ingenuity Blade Station 8 Airfoil, r/R = 0.9912

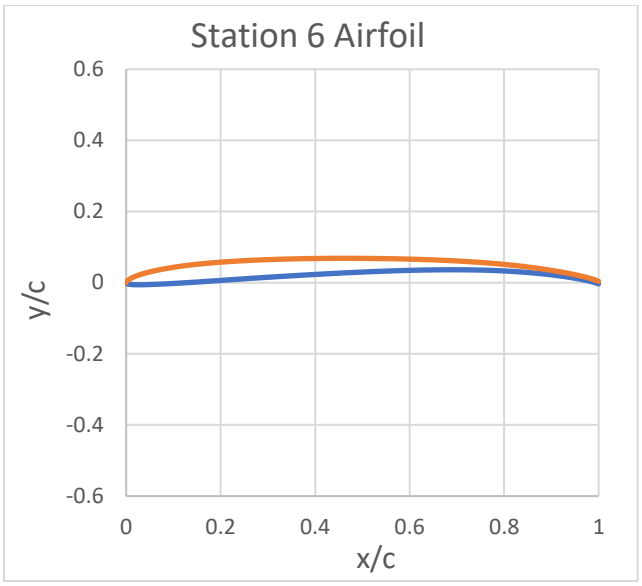

Figure 3: Ingenuity Blade Station 6 Airfoil, r/R = 0.7620

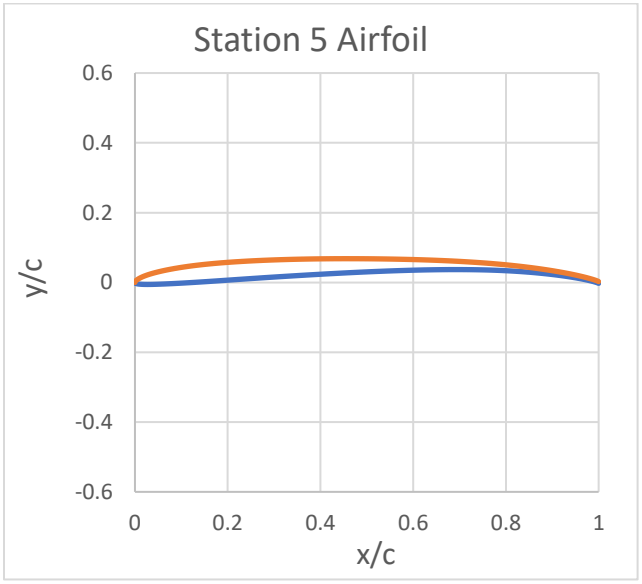

Figure 4: Ingenuity Blade Station 5 Airfoil, r/R = 0.5271

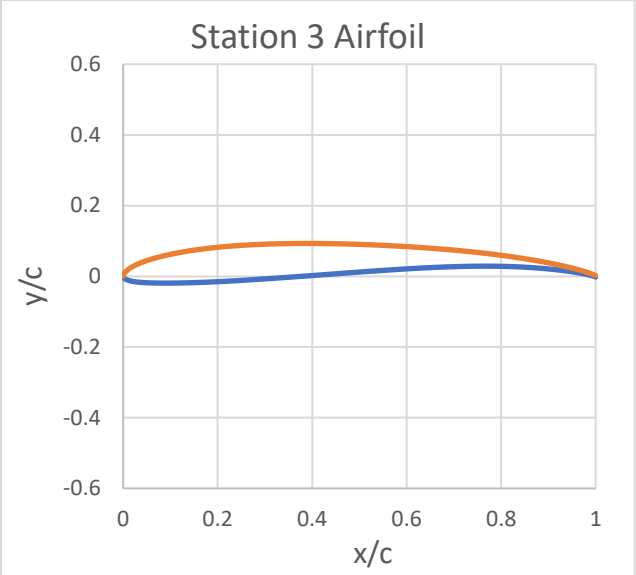

Figure 5: Ingenuity Blade Station 3 Airfoil, r/R = 0.2950

Grids were generated using Chimera Grid Tools 2.2 (CGT) and the gridding guidelines from the American Institute of Aeronautics and Astronautics (AIAA) CFD High Lift Prediction Workshop were used where applicable [16,17]. The (2D) grid size is based on the grid resolution study (GRS) at alpha = 4° (approximate outboard angle of attack in hover for Ingenuity) at conditions corresponding to radial stations r/R = 0.50, 0.75, and 0.90 [13].

The grid is generated to anticipate thick boundary layers and unsteady separated shear layer behavior because of the low Reynolds numbers experienced by the rotor. As such, the maximum chordwise and off-body separation was fixed at 0.5%c in the predominant region of unsteady separated flow (up to 0.20c off-body), as shown in red in Figure 6. The y+ value is kept at unity for all grids and the farfield was set at 200c, as shown in Figure 7. For further detailed information on the grid generation, the process is referred to in Reference 7.

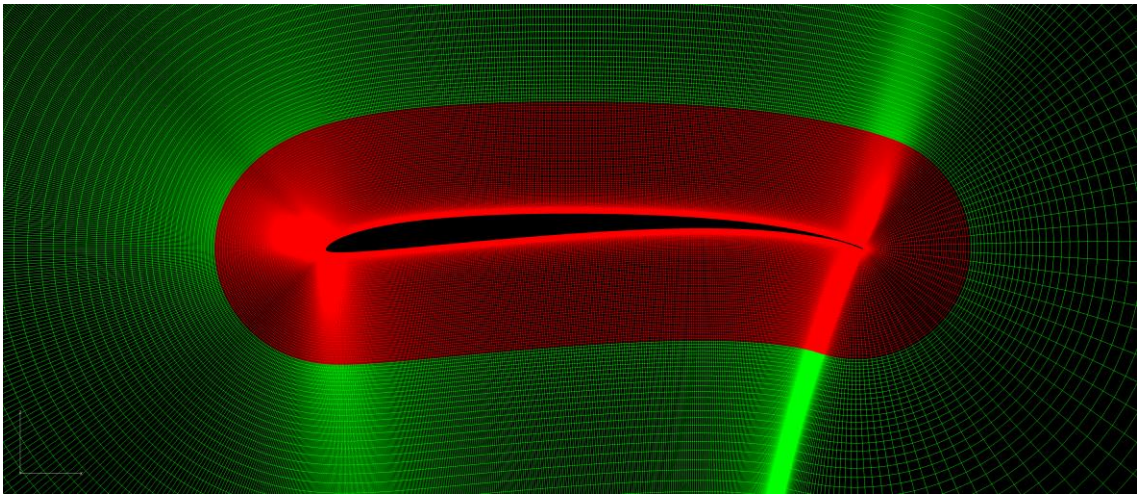

Figure 6: Nearbody Grid, Showing the Red Refinement Region with Maximum Global Spacing

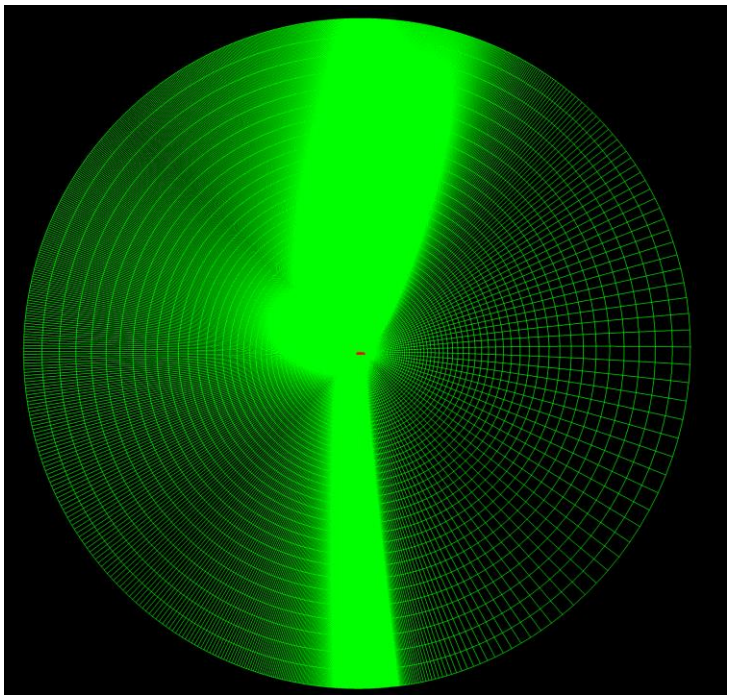

Figure 7: Farfield Grid

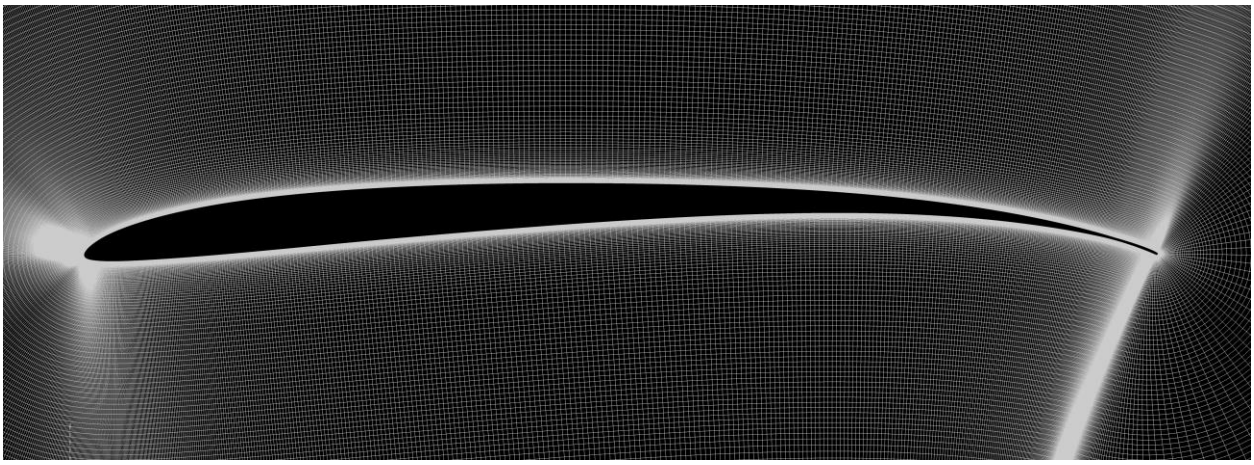

Figure 8: Detailed View of the Nearbody Grid

Along with the airfoils at the particular radial stations, the Ingenuity blades were defined by the twist and chord as a function of radial station. The blades have maximum twist and maximum chord at approximately quarter span and then reduce in twist and chord toward the tip of the blade. The Ingenuity blade chord and twist distributions are shown in Figure 9 and Figure 10. Similar to the airfoils discussed above, the chord and twist distribution data is obtained from the as-built blades rather than the original designs. The tabulated data for the geometry of the Ingenuity blade is provided in Table 1.

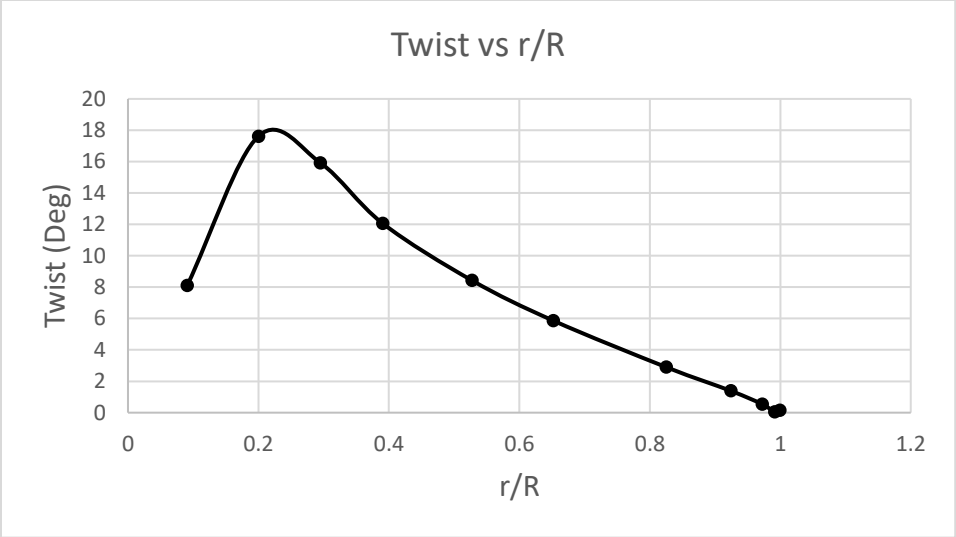

Figure 9: Ingenuity Blade Twist Distribution

Figure 10: Ingenuity Blade Chord Distribution

Table 1: Ingenuity Blade Tabulated Airfoil Data

Station	Airfoil Name	Radial Station (r/R)	Chord (mm)	Thickness/Chord (%)	Airfoil Deck Modification
1	Station 1	0.091	26.4	96.2	None
2	Station 2	0.200	85.1	22.0	None
3	Station 3	0.295	119.1	9.8	None
4	Station 4	0.390	119.1	5.9	Modified
5	CLF5605	0.527	98.4	5.0	Modified
6	CLF5605	0.762	73.2	5.0	Modified
7	CLF5605	0.924	52.0	5.0	Modified
8	CLF5605	0.991	20.6	5.0	Modified

Modification of Airfoil Decks

Modification of Angle of Attack Values

To capture the behavior of the various airfoils in the Ingenuity blades, C81 tables, a type of airfoil performance table which describes c_l, c_d, and c_m as a function of angle of attack at various Mach numbers, were used. The original CAMRAD II analysis of the EDM1 tests used unmodified C81 tables of Ingenuity airfoils obtained using the process described above. Eight C81 tables were used to describe the eight airfoils used in the Ingenuity blade design described previously. For all three densities, the results obtained from CAMRAD II analysis using the unmodified tables yielded C_T/σ vs collective slopes that were too steep, shown in Figure 11 through Figure 13.

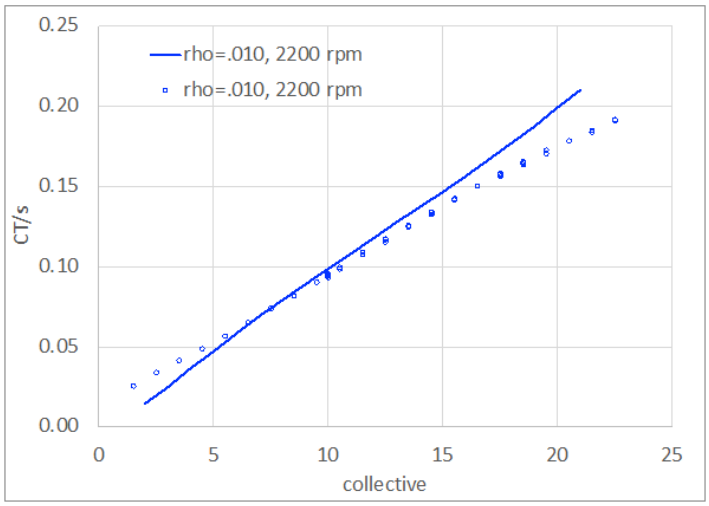

Figure 11: EDM1 (Points) and Original CAMRAD II Results (Solid) for 0.01 Density

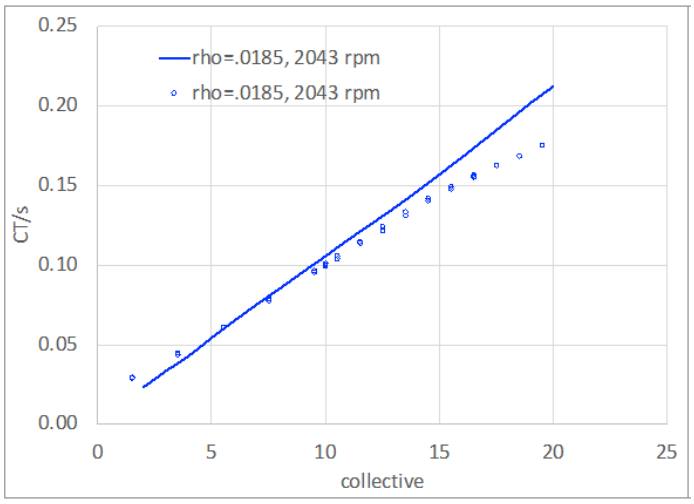

Figure 12: EDM1 (Points) and Original CAMRAD II Results (Solid) for 0.0185 Density

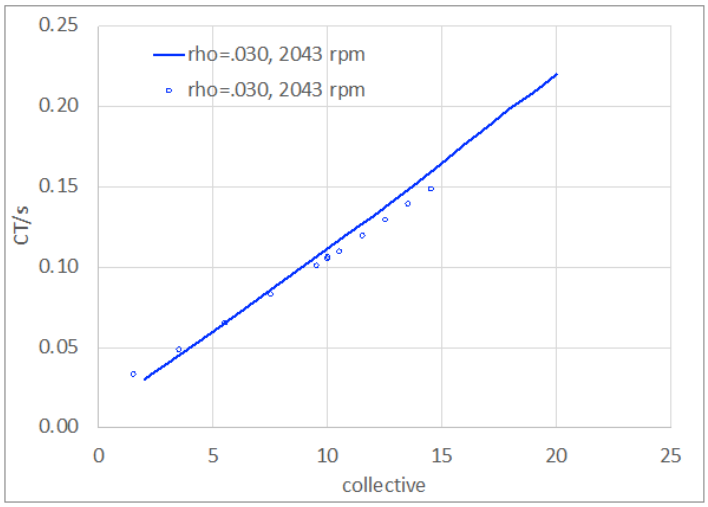

Figure 13: EDM1 (Points) and Original CAMRAD II Results (Solid) for 0.03 Density

Figure 11 through Figure 13 show that CAMRAD II results using the original airfoil tables consistently underpredict C_T/σ at collective values below approximately 5 degrees and overpredict C_T/σ at higher collective angles. To reduce the slope of the C_T/σ vs collective curve for the CAMRAD II results, angle of attack values were increased in the C81 table while leaving the coefficient values unchanged. The effect of this modification is to effectively provide lower c_l, c_d, and c_m values over a wider range of angles of attack. An example of these changes is shown in Figure 14.

To prevent sharp, unrealistic changes in c_l, c_d, or c_m versus angle of attack, only angle of attack values between -15 and 20 degrees were modified. In this range of angle of attack values, c_l, c_d, and c_m data is unique to the Ingenuity airfoils used . Data outside of this range is populated with NACA 0012 data. The method of modification was both multiplicative and additive for the range of modified angles of attack. Higher values of the multiplication factor decreases the slope of the curve due to a greater spread in the angle of attack values, while subtraction shifts the entire curve higher as higher c_l values are reached at lower angles of attack. This behavior can be seen in Figure 14 where a multiplicative factor of 1.5 is too shallow, while a factor of 1.1 brings the CAMRAD II values closer to the experimental values. Several iterations of CAMRAD II calculations were performed with different modification equations at the three densities before determining the final modification.

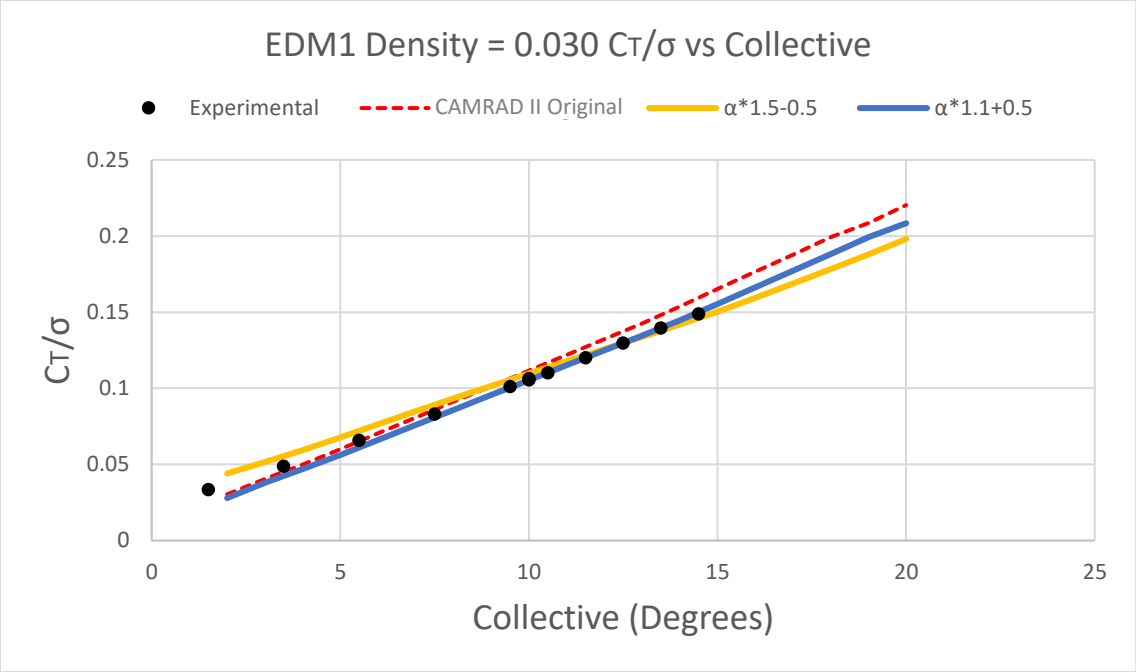

Figure 14: Sample C_T/σ vs Collective Plots with Modified Angle of Attack Values at 0.03 Density

The modification of the angle of attack values that achieved C_T/σ vs collective curves that most closely matched the experimental values for all three densities was using a multiplication factor of 1.2 with no addition. While this modification did not perfectly fit the experimental data, it had an improved fit for all three densities, and had especially good fit in the 10-15 degree collective range, which was the region of most interest for predicting operational performance. The final C_T/σ vs collective curves for all three EDM1 densities are shown in Figure 15 through Figure 17.

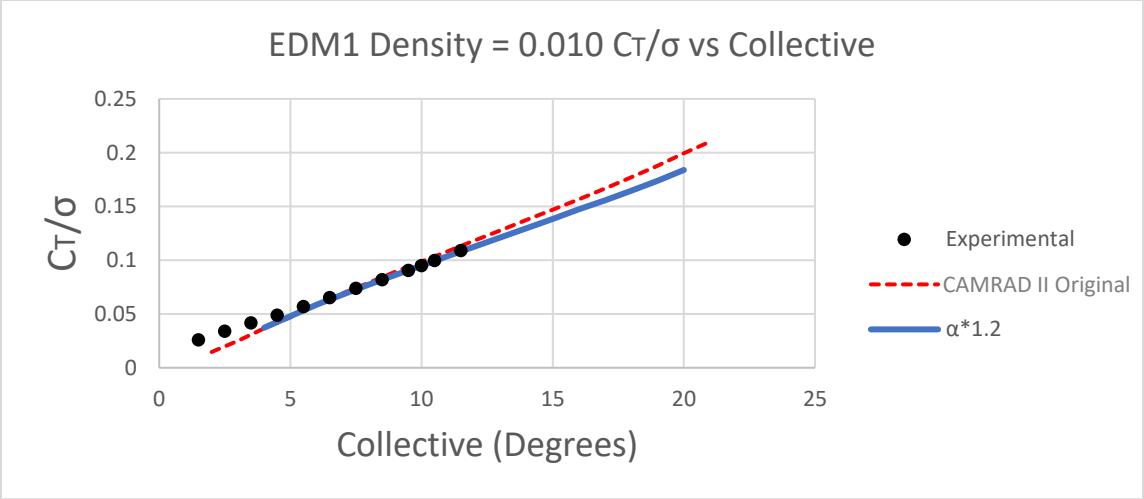

Figure 15: C_T/σ vs Collective at 0.01 Density for EDM1, Original CAMRAD II, and 1.2 Multiplied Angle of Attack

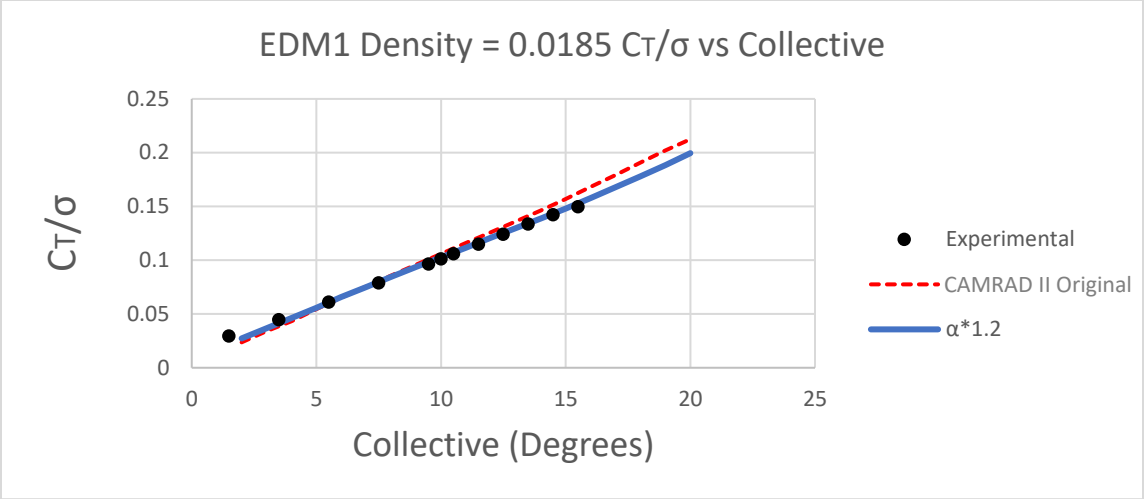

Figure 16: C_T/σ vs Collective at 0.0185 Density for EDM1, Original CAMRAD II, and 1.2 Multiplied Angle of Attack

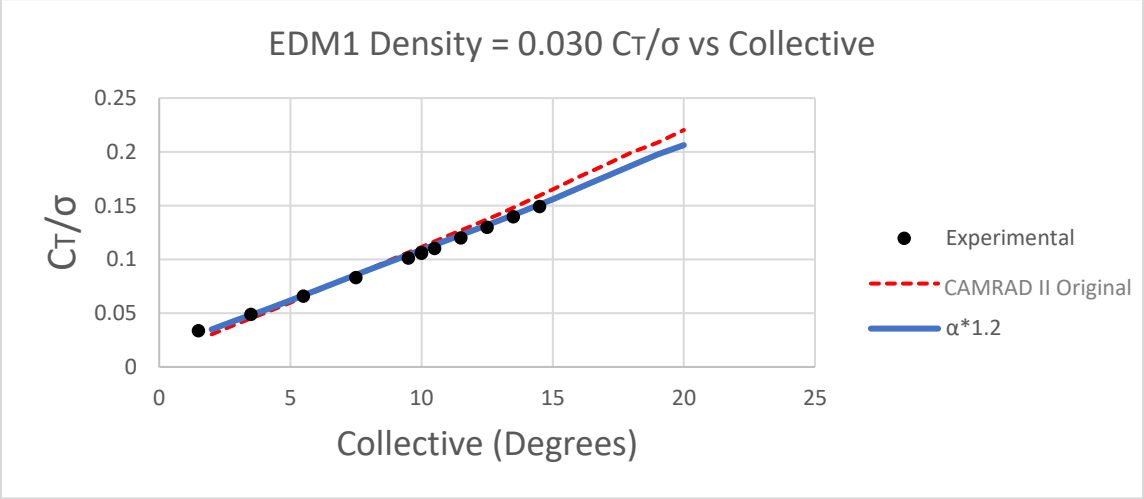

Figure 17: C_T/σ vs Collective at 0.03 Density for EDM1, Original CAMRAD II, and 1.2 Multiplied Angle of Attack

Similar work with modification of angle of attack values was performed for the TRT results. While a single equation was able to closely match experimental C_T/σ vs collective data for all three densities in the EDM1 results, a single equation was not usable for the various rotational speeds in the TRT results. The original CAMRAD II C_T/σ vs collective data had a steady increase in slope with increasing tip Mach number, requiring larger multiplication factors for higher RPM cases. While the EDM1 results did not require an additive factor, the TRT results did require additive factors to properly shift the curve with the correct slope to align with the experimental data. The angle of attack multiplication factors that worked best for the RPMs in increasing order were 1.2, 1.4, 1.5, 1.6, and 1.8 respectively with additive factors of -1, -1, -2.5, -2.5, and -2.5. The plots of the experimental data and the respective CAMRAD II results for each RPM are shown in Figure 18 through Figure 22.

The difference in slope of thrust as a function of collective for the two tests is likely associated with differences in aerodynamics of coaxial and single rotors, and especially differences in the hub and control system of the two test stands. The thrust/collective slope dependence on RPM suggests that the behavior is due to inertial and mechanical effects more than aerodynamics.

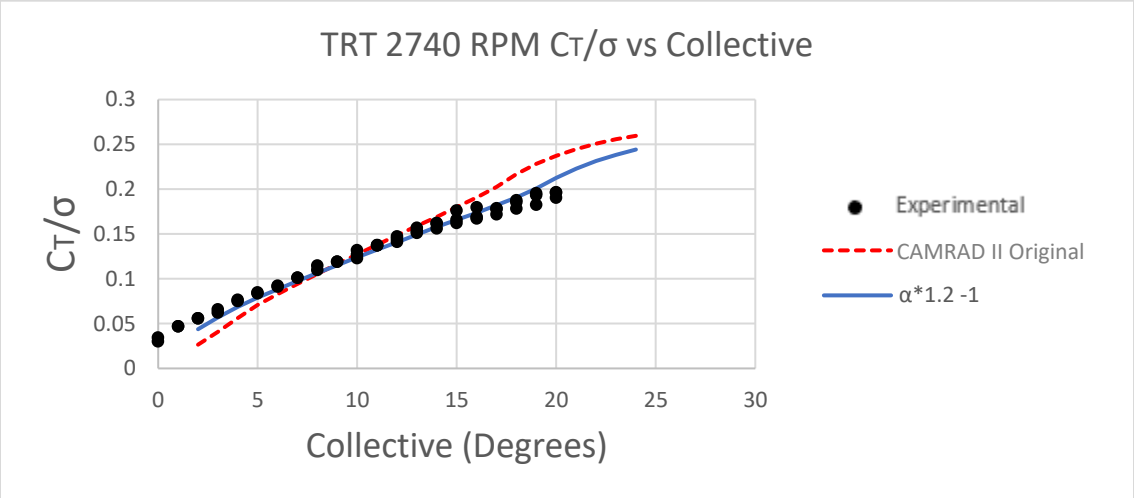

Figure 18: TRT 2740 RPM C_T/σ vs Collective Modification

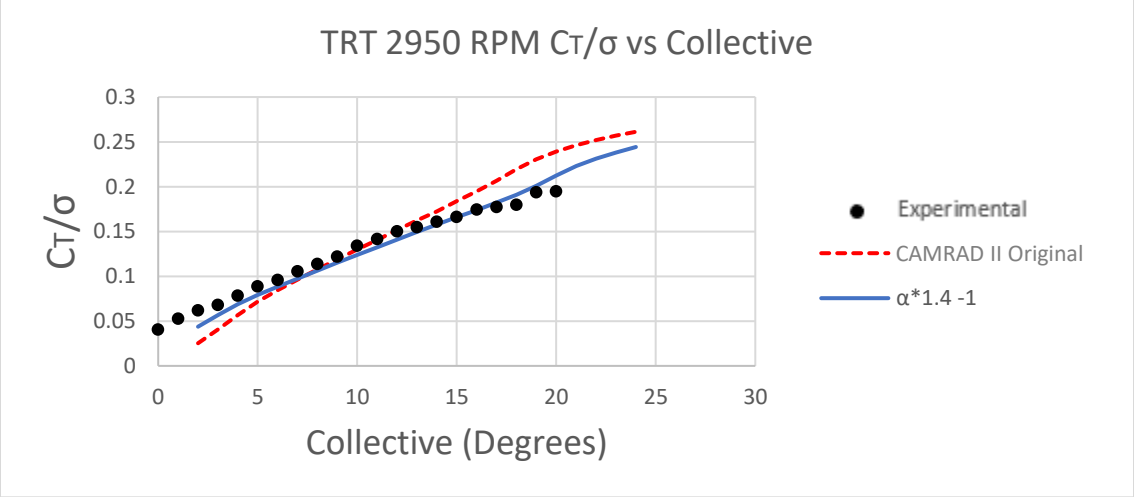

Figure 19: TRT 2950 RPM C_T/σ vs Collective Modification

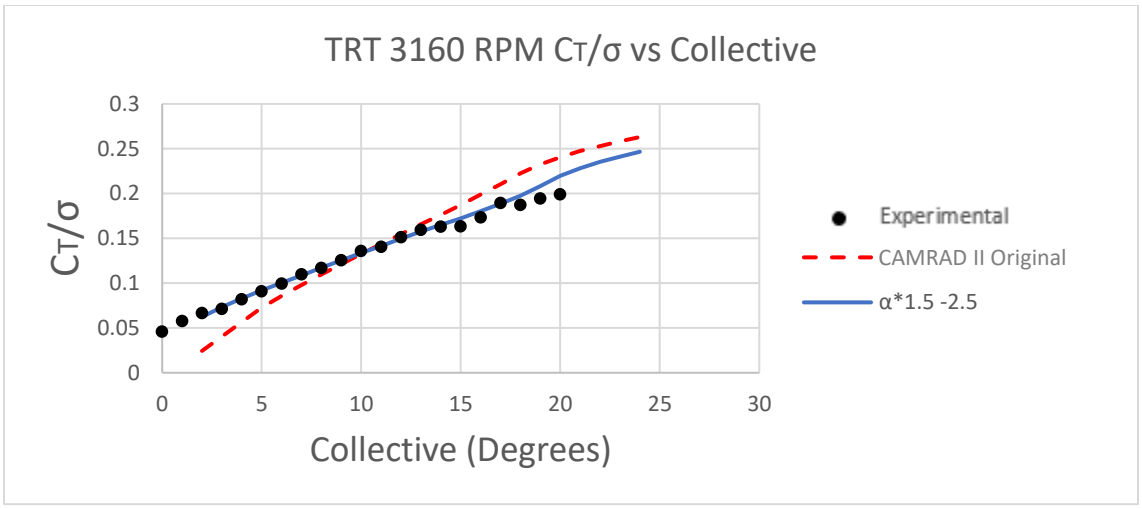

Figure 20: TRT 3160 RPM C_T/σ vs Collective Modification

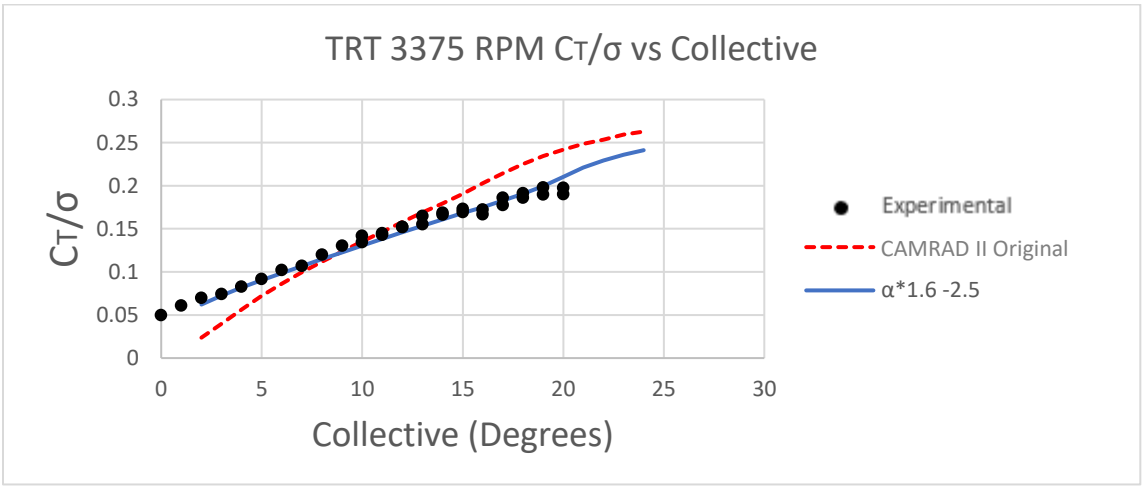

Figure 21: TRT 3375 RPM C_T/σ vs Collective Modification

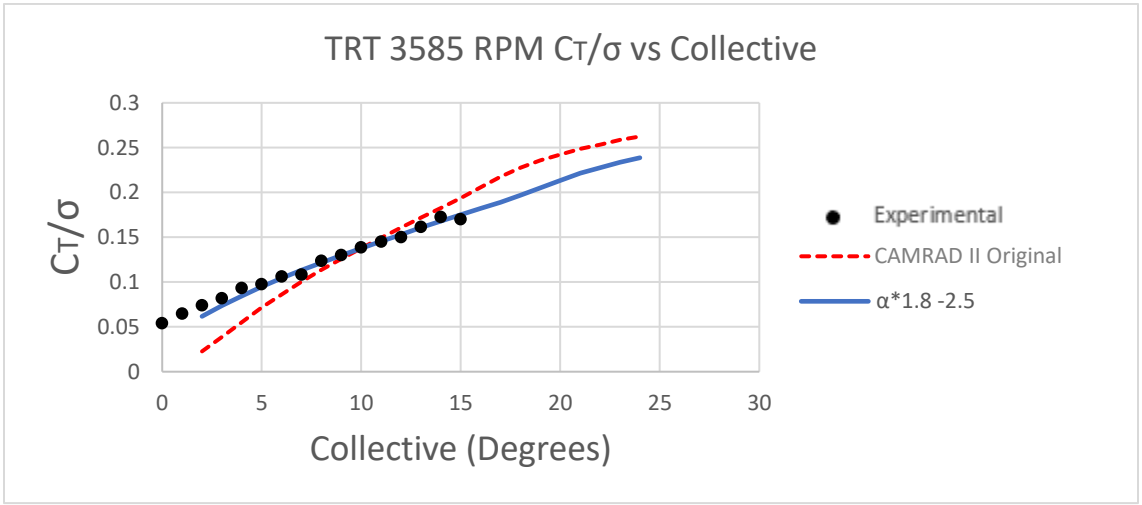

Figure 22: TRT 3585 RPM C_T/σ vs Collective Modification

To ensure that the modifications were not creating unrealistic changes to the airfoil decks, c_l, c_d, and c_m were all plotted vs angle of attack for all blade stations for each of the densities. Since the angles of attack were only scaled, and by only 1.2, the plots were expectedly smooth and realistic, with no sudden changes in value or unrealistic values. The only sudden changes in c_l, c_d, and c_m values are at the boundary between the airfoil data specifically for the Ingenuity blades and the NACA 0012 data used for angle of attack values beyond the operation range of Ingenuity. An example of the changes in the airfoil tables is provided in Figure 23, showing c_l vs angle of attack for the density of 0.01 kg/m^3 and radial station 6 at various Mach numbers. All modified c_l, c_d, and c_m vs angle of attack plots similarly exhibited a stretching about the angle of attack with no other changes. Additive factors used for the TRT CAMRAD II results simply resulted in a shift as well as the stretch resulting from the multiplicative factor.

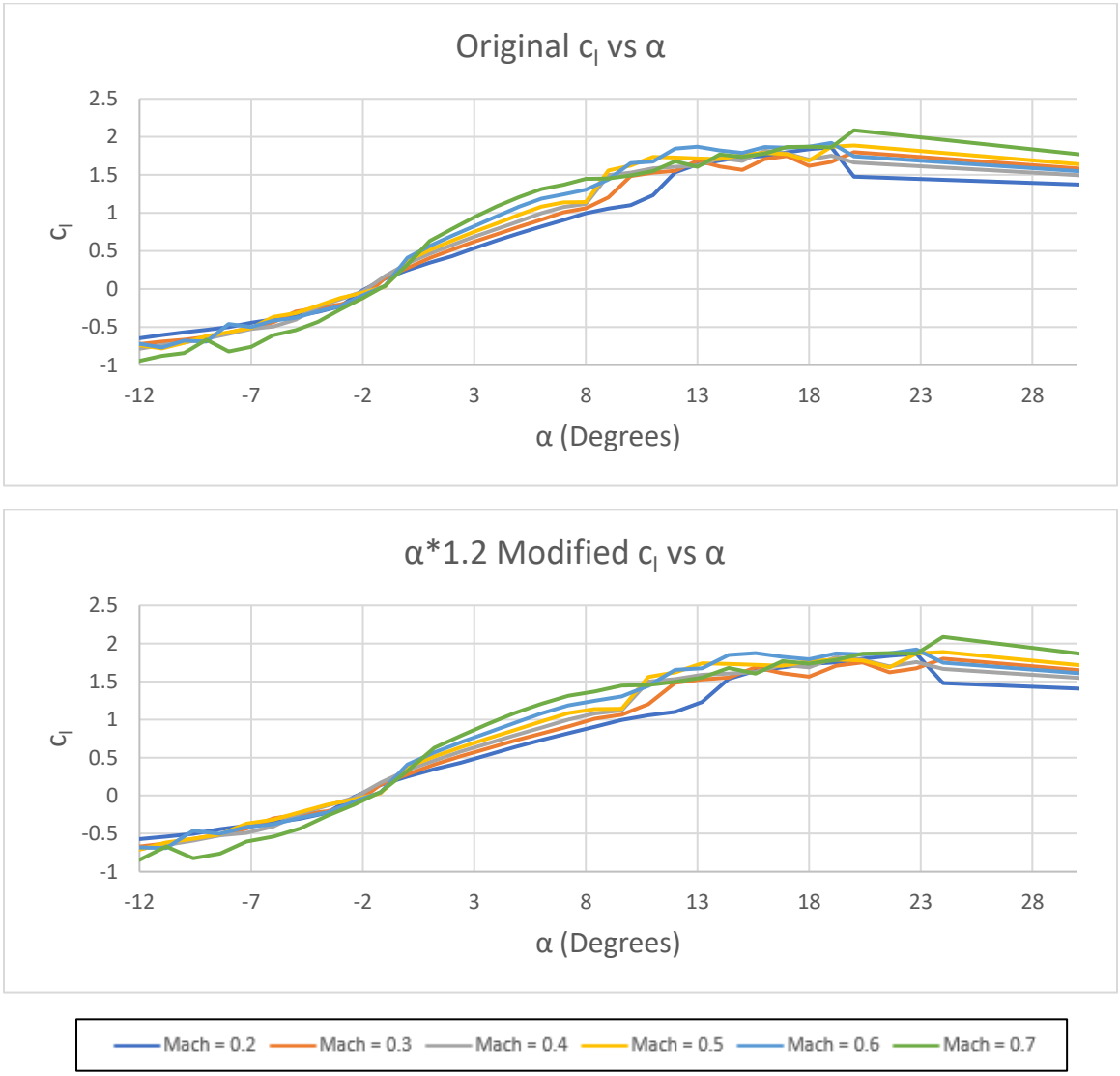

Figure 23: c_l vs Angle of Attack Comparison for Original Airfoil Tables (Top) and Modified Airfoil Tables with Angle of Attack Multiplied by 1.2 (Bottom) (Radial Station 6, Density =0.01 kg/m^3)

Modification of Coefficient of Drag Values

While modification of the angles of attack values brought C_T/σ vs collective CAMRAD II results closer to the experimental results for EDM1 and TRT, further work was required to correct for FM vs C_T/σ and C_P vs C_T discrepancies. These results are especially problematic as they predict higher figure of merit and better performance rather than providing conservative estimates. To predict performance more accurately and conservatively, the c_d values in the airfoil tables were also modified to increase by an increment that changed at different angle of attack values.

To maintain the more accurate C_T/σ vs collective relationship, all airfoil tables retained the multiplied angle of attack values between -15 and 20 degrees. Based on similar work to reconcile Helicat predictions and EDM1 data at the Jet Propulsion Laboratory, an exponential modification was used with the form

$$c_d' = c_d + k * (\alpha - \alpha_{ref})^x$$

where k and x values determine what value is added to the original c_d value based on the difference between the angle of attack and an arbitrary reference angle of attack, α_{ref}, where the modification begins [3]. Any c_d values with an angle of attack below the reference value were not modified and the c_d values were only modified up to 24 degrees. The upper limit of 24 degrees is used since the upper limit of the unmodified angle of attack values was 20 degrees. After multiplication of angle of attack values, this upper limit becomes 24 degrees.

The first iteration of these modifications focused on finding a single c_d modification that would work for all three EDM1 test densities. While several modifications were found for each density that aligned closely with experimental data, no single modification could be found that matched experimental data for the whole range of C_T/σ and C_T in the respective plots. To further constrain the results, the same process was performed, while focusing mainly on the C_T/σ range of 0.1 to 0.15. The final values used for this modification were k = 0.001, α_{ref} = 2.0, and x = 2.3. The results are also shown in Figure 24 through Figure 29.

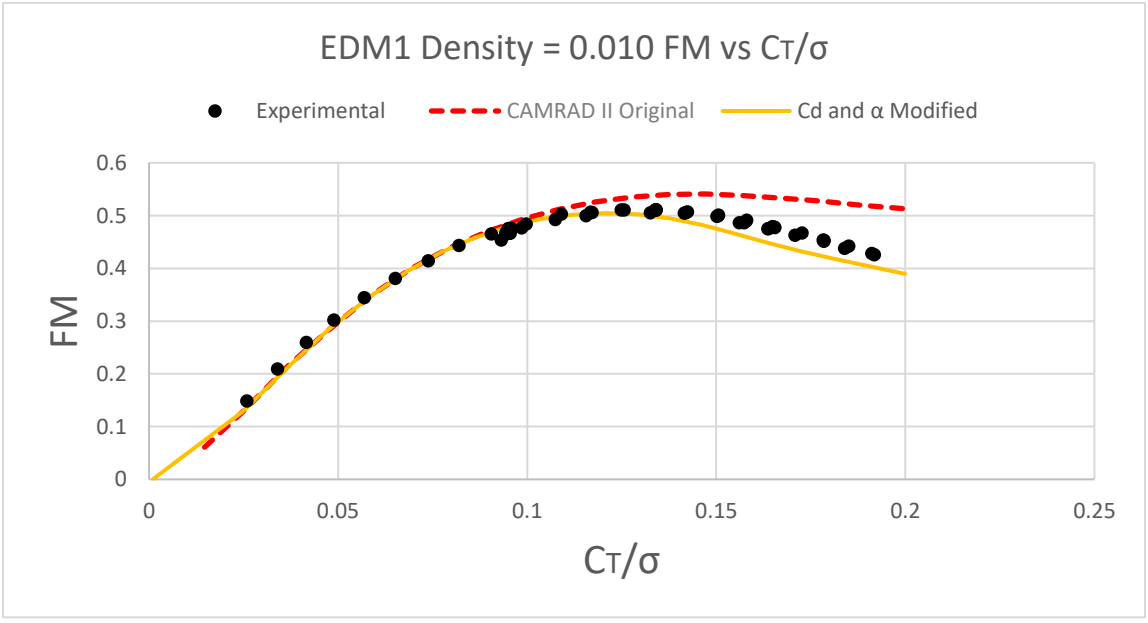

Figure 24: 0.01 Density FM vs C_T/σ Results with CAMRAD II Results Using Modification of c_d values with Angle of Attack Multiplication

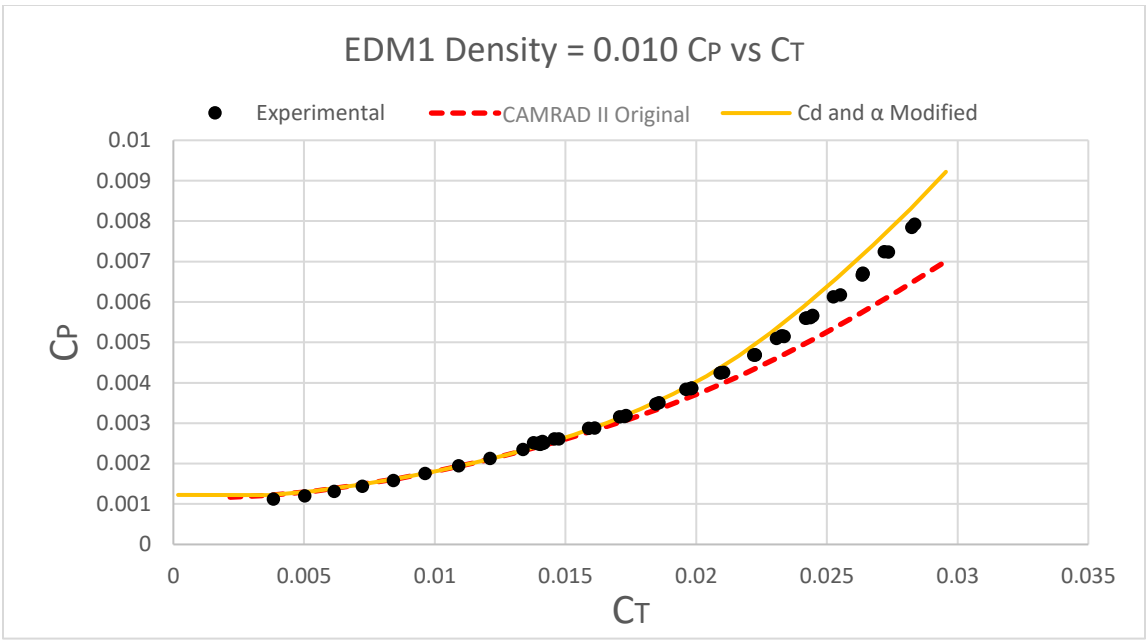

Figure 25: 0.01 Density C_P vs C_T Results with CAMRAD II Results Using Modification of c_d values with Angle of Attack Multiplication

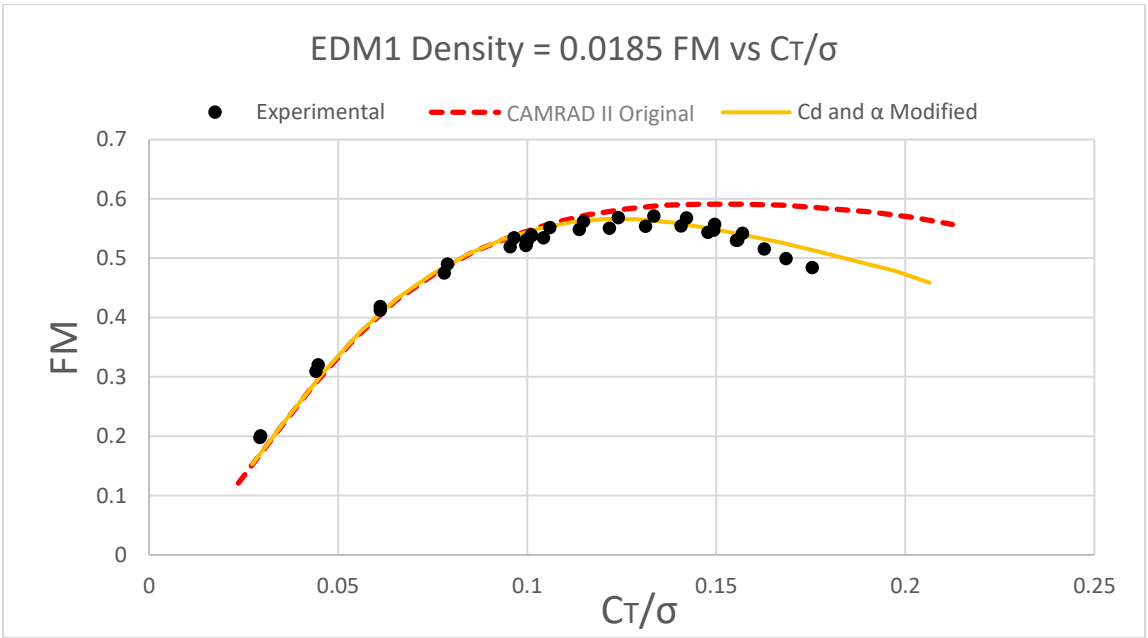

Figure 26: 0.0185 Density FM vs C_T/σ Results with CAMRAD II Results Using Modification of c_d values with Angle of Attack Multiplication

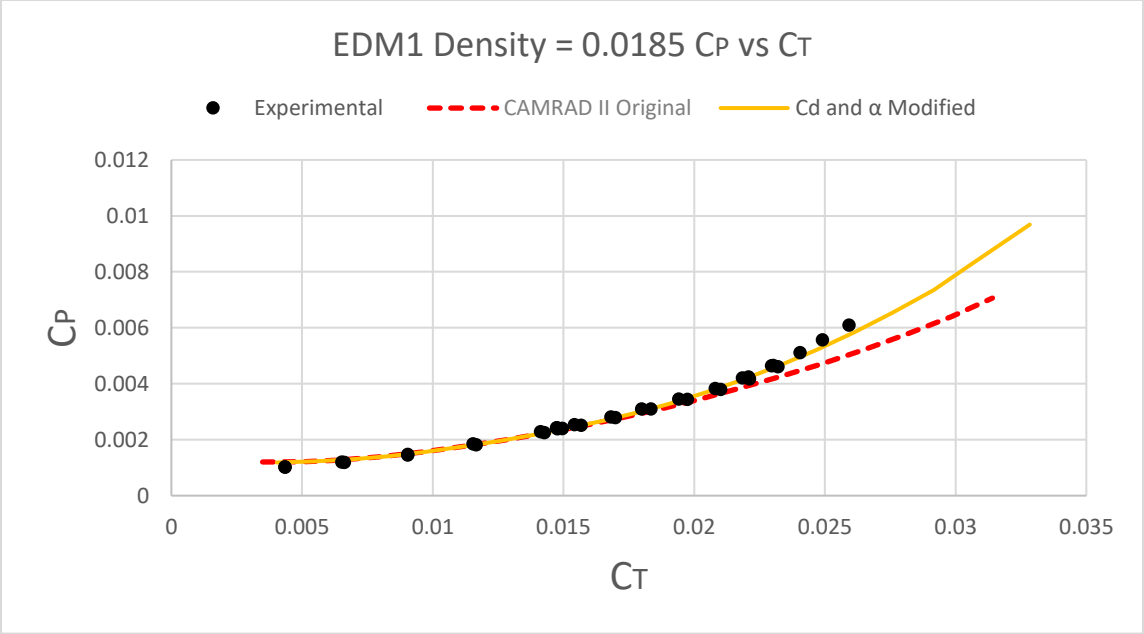

Figure 27: 0.0185 Density C_P vs C_T Results with CAMRAD II Results Using Modification of c_d values with Angle of Attack Multiplication

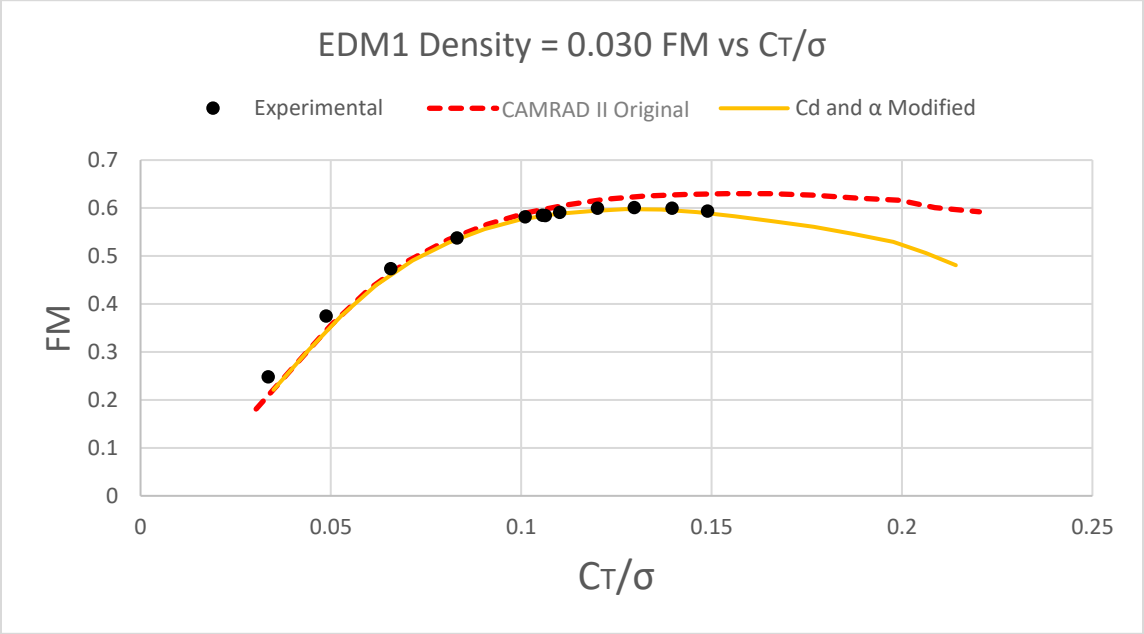

Figure 28: 0.03 Density FM vs C_T/σ Results with CAMRAD II Results Using Modification of c_d values with Angle of Attack Multiplication

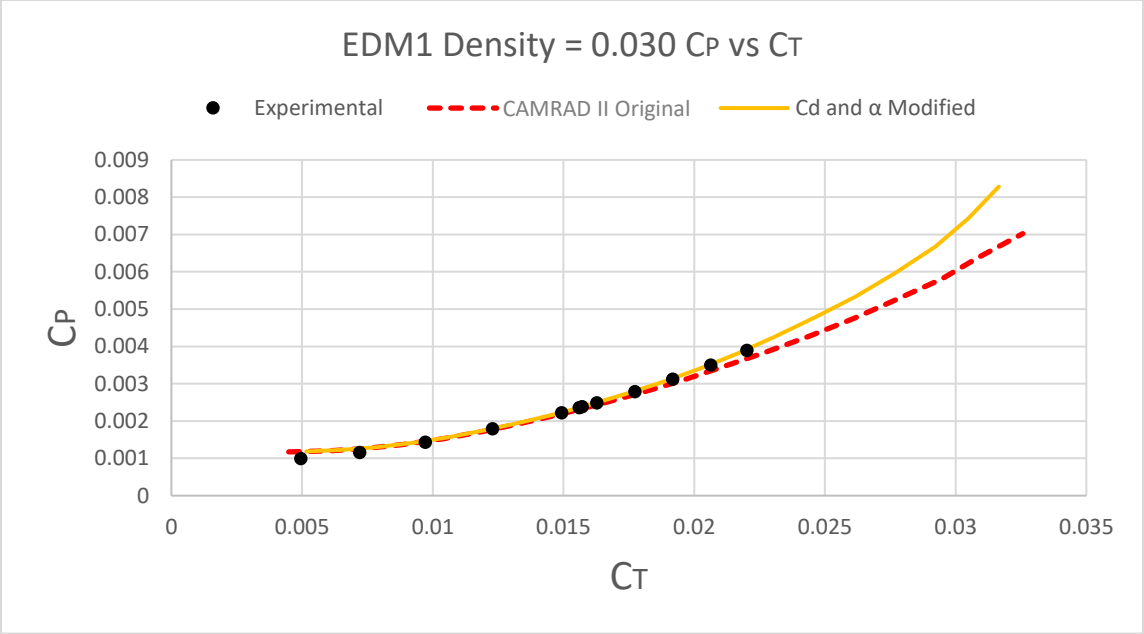

Figure 29: 0.03 Density C_P vs C_T Results with CAMRAD II Results Using Modification of c_d values with Angle of Attack Multiplication

While this initial modification of the c_d values provided more accurate and conservative performance predictions, especially in the $0.1 < C_T/\sigma < 0.15$ range, the predictions were consistently conservative relative to experimental results at C_T/σ values below 0.075. This consistent underprediction was a result of limiting the c_d modification to angles of attack above 2 degrees. To improve the correlation at low C_T/σ values, the c_d modification was altered to now include four distinct ranges, following the behavior:

$$c'_d = c_d + \begin{cases} -k * \left|\alpha_{ref,1} - \alpha_{ref,2}\right|^x, & -15 < \alpha < \alpha_{ref,1} \\ -k * \left|\alpha - \alpha_{ref,2}\right|^x, & \alpha_{ref,1} < \alpha < \alpha_{ref,2} \\ +k * \left|\alpha - \alpha_{ref,2}\right|^x, & \alpha_{ref,2} < \alpha < \alpha_{ref,3} \\ +k * \left|\alpha_{ref,3} - \alpha_{ref,2}\right|^x, & \alpha_{ref,3} < \alpha < 20 \end{cases}$$

where k and x operate similar to the previous modification, but in four distinct ranges, requiring three different reference angles of attack, where $\alpha_{ref,1} < \alpha_{ref,2} < \alpha_{ref,3}$. This modification is only performed in the range of -15 to 20 degrees before modification of angle of attack values, since this is the region where data is unique to the Ingenuity blades, and where NACA 0012 values are not used. The additive c_d increment as a function of angle of attack is shown in Figure 30.

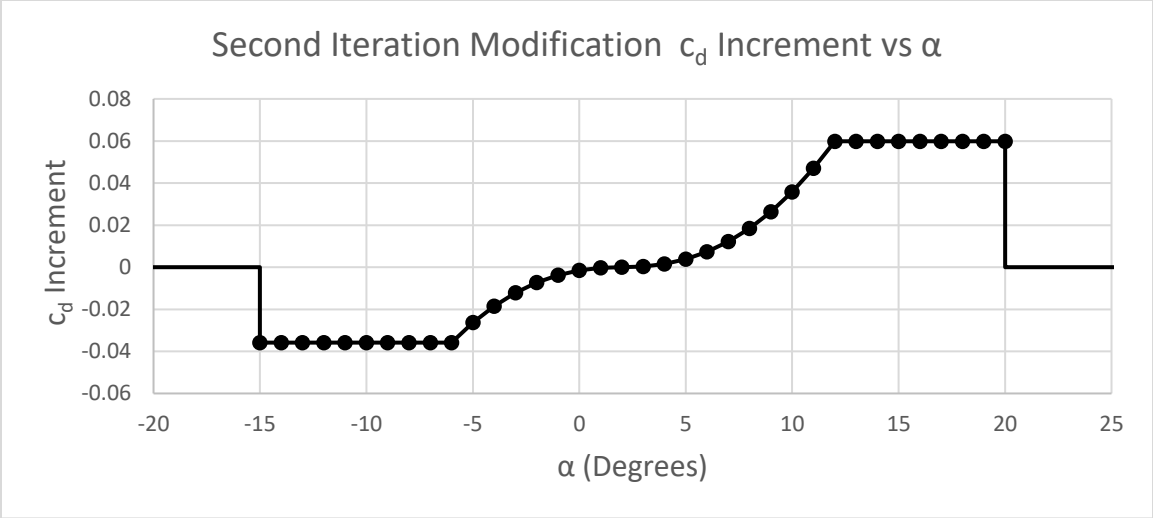

Figure 30: c_d Increment vs Angle of Attack for Final EDM1 Airfoil Table Modification

This method of modification offers additional ability to refine the results for a wider range of C_T/σ values while maintaining the correct C_T/σ to collective relationship. However, to fully implement the modifications to capture low C_T/σ values, additional collective values were needed in the CAMRAD II analysis. The new range of collective sweep in CAMRAD II used was -4 to 24. In addition to the expanded collective range, the angle of attack modification was no longer used specifically for the c_d portions of the airfoil tables. This was done so that angle of attack and c_d modification did not have compounding effects on the performance. Angle of attack modification was still performed for c_l and c_m in order to accurately capture the C_T/σ vs collective behavior. The combination of values that captured the full range of FM vs C_T/σ and C_P vs C_T behavior best for all three densities was k = 0.0003, x = 2.3, $\alpha_{ref,1}$ = -6 degrees, $\alpha_{ref,2}$ = 2 degrees, and $\alpha_{ref,3}$ = 12 degrees. The EDM1 CAMRAD II results with these modifications are provided in Figure 31 through Figure 36.

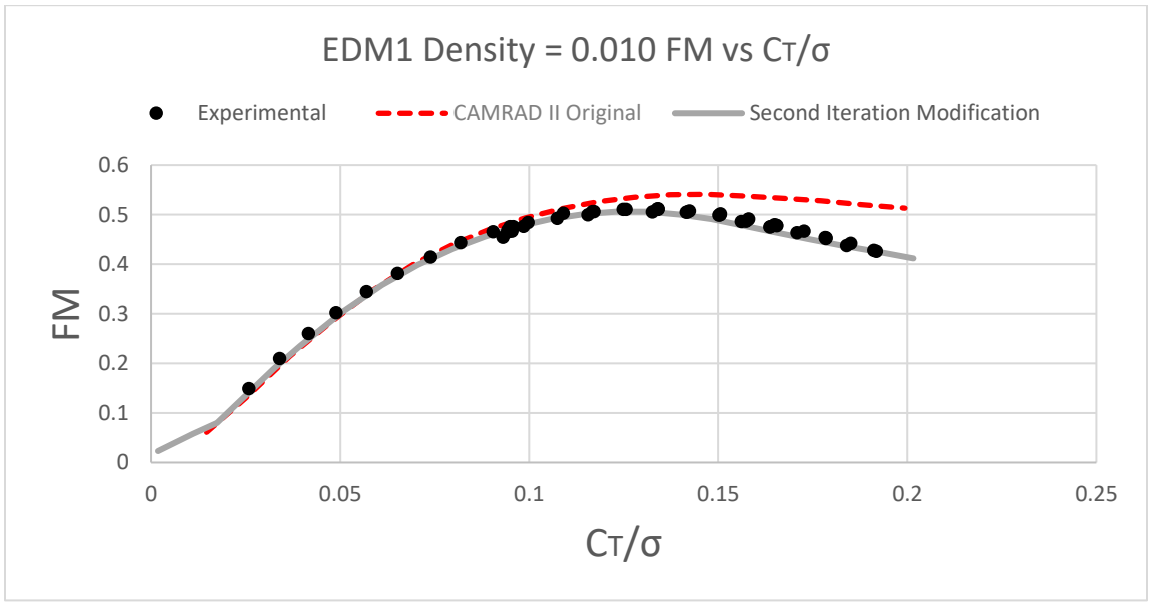

Figure 31: 0.01 Density FM vs C_T/σ Results with CAMRAD II Results with Second Iteration Airfoil Table Modification

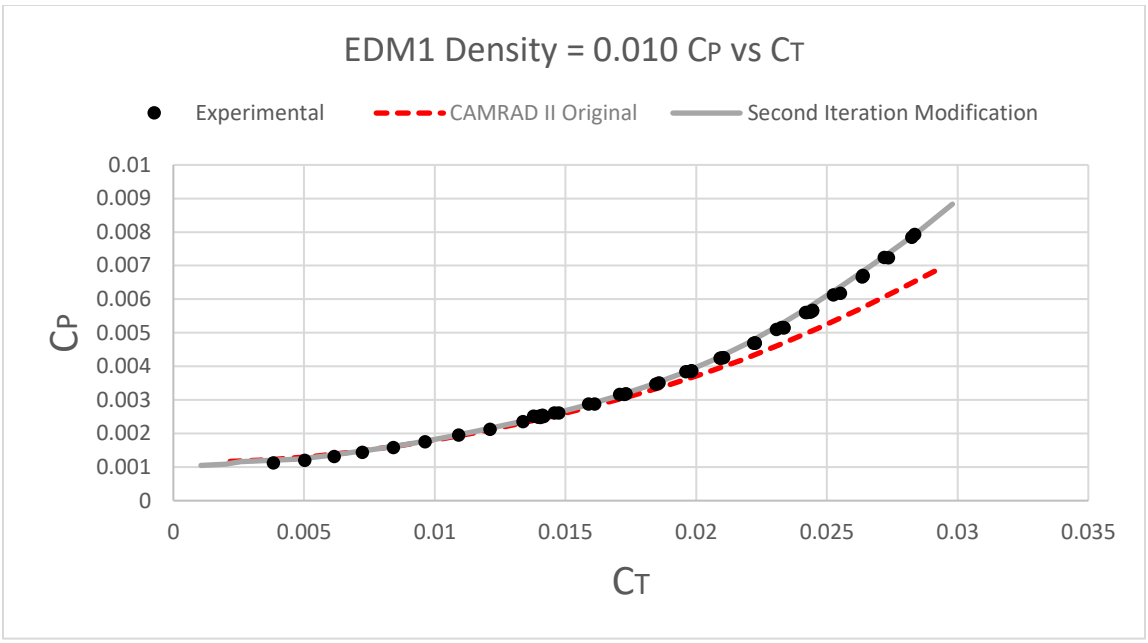

Figure 32: 0.01 Density C_P vs C_T Results with CAMRAD II Results with Second Iteration Airfoil Table Modification

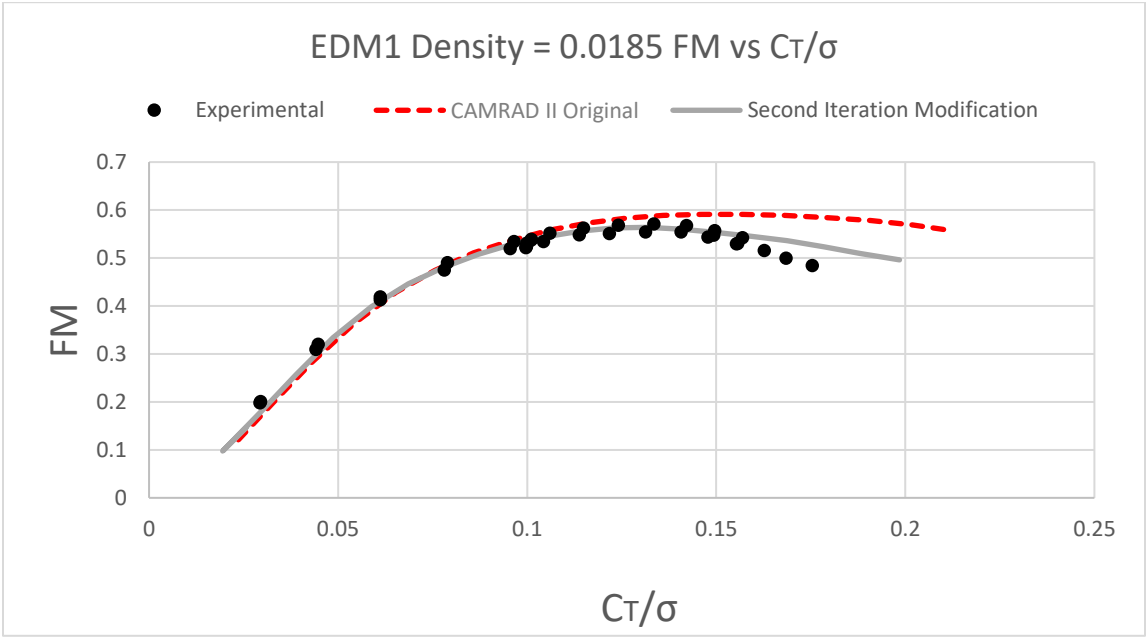

Figure 33: 0.0185 Density FM vs C_T/σ Results with CAMRAD II Results with Second Iteration Airfoil Table Modification

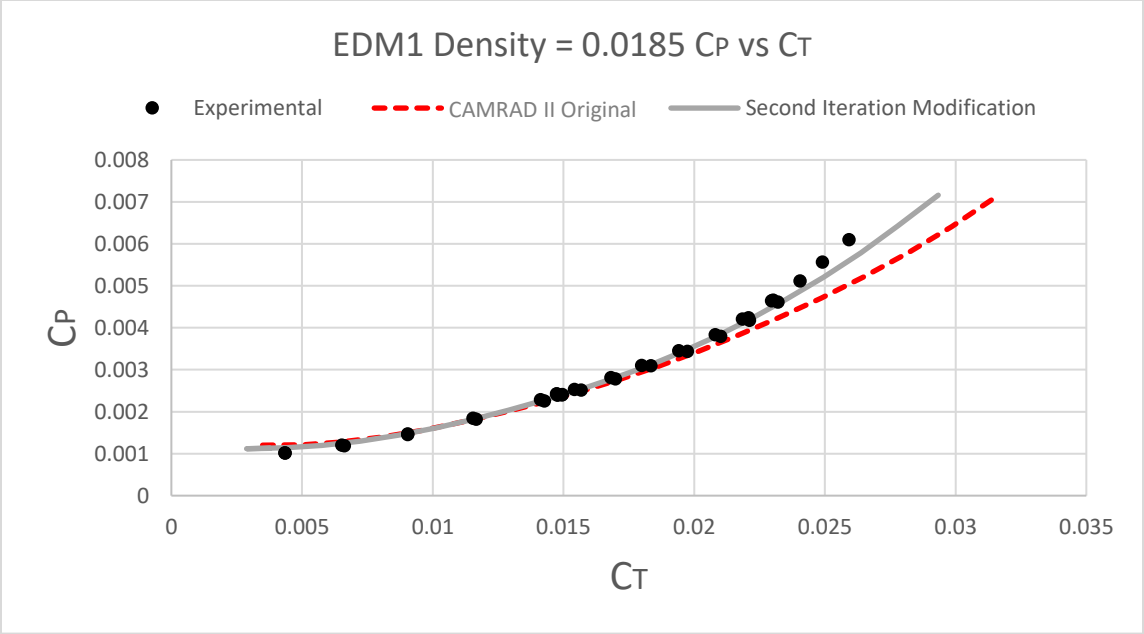

Figure 34: 0.0185 Density C_P vs C_T Results with CAMRAD II Results with Second Iteration Airfoil Table Modification

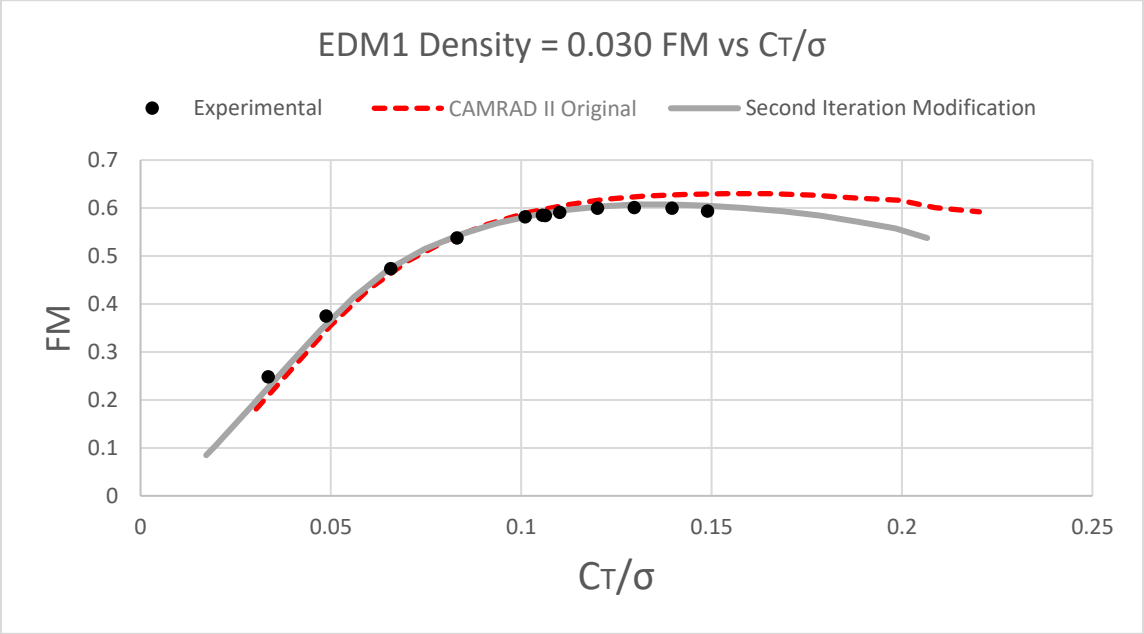

Figure 35: 0.03 Density FM vs C_T/σ Results with CAMRAD II Results with Second Iteration Airfoil Table Modification

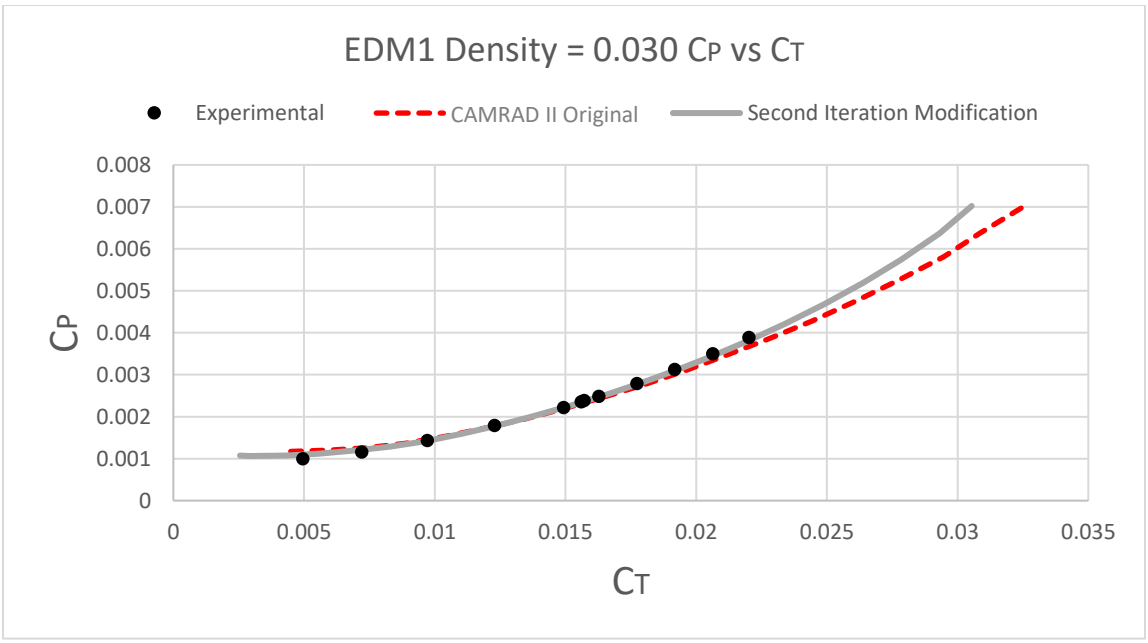

Figure 36: 0.03 Density C_P vs C_T Results with CAMRAD II Results with Second Iteration Airfoil Table Modification

The second iteration of c_d modification allows for accurate and conservative predictions of EDM1 data. There are some remaining non-conservative predictions, mainly at C_T/σ values greater than 0.15, but the predictions in the C_T/σ range of 0.1 to 0.15 are within 5% of experimental values. The C_P error versus C_T/σ plots for all three EDM1 densities using the final modified CAMRAD II results are provided in Figure 37 through Figure 39.

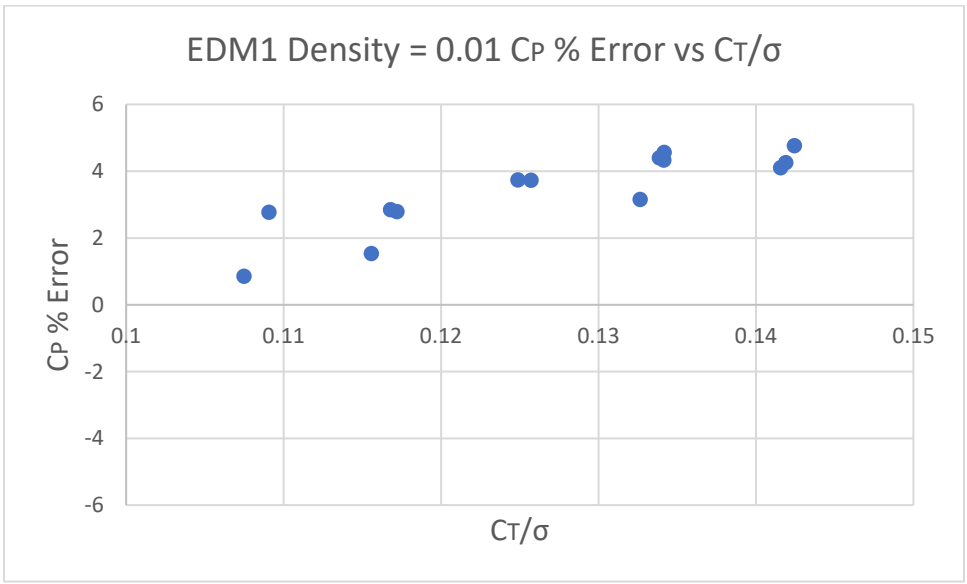

Figure 37: C_P % Error vs C_T/σ for Density = 0.01 EDM1 Results and Final Modified CAMRAD II Results

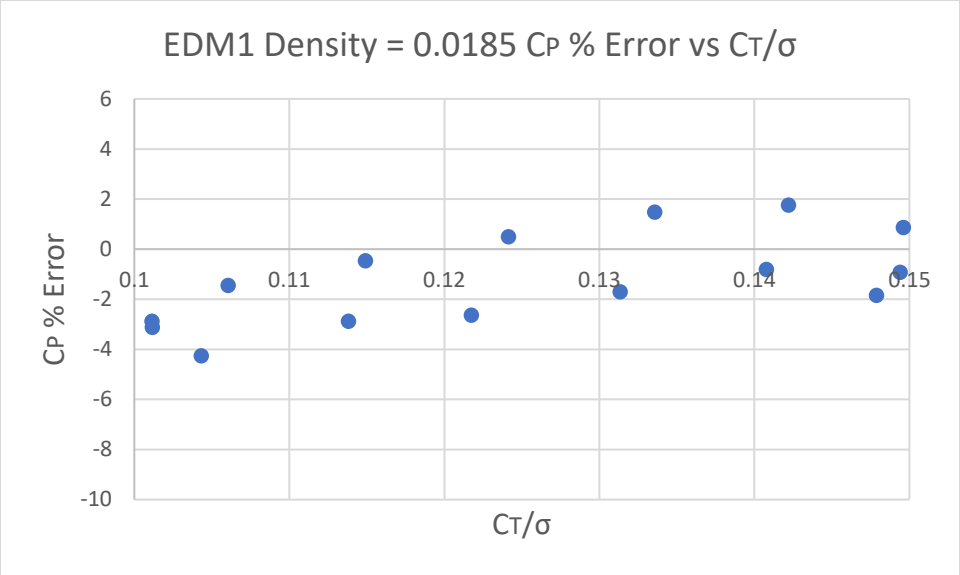

Figure 38: C_P % Error vs C_T/σ for Density = 0.0185 EDM1 Results and Final Modified CAMRAD II Results

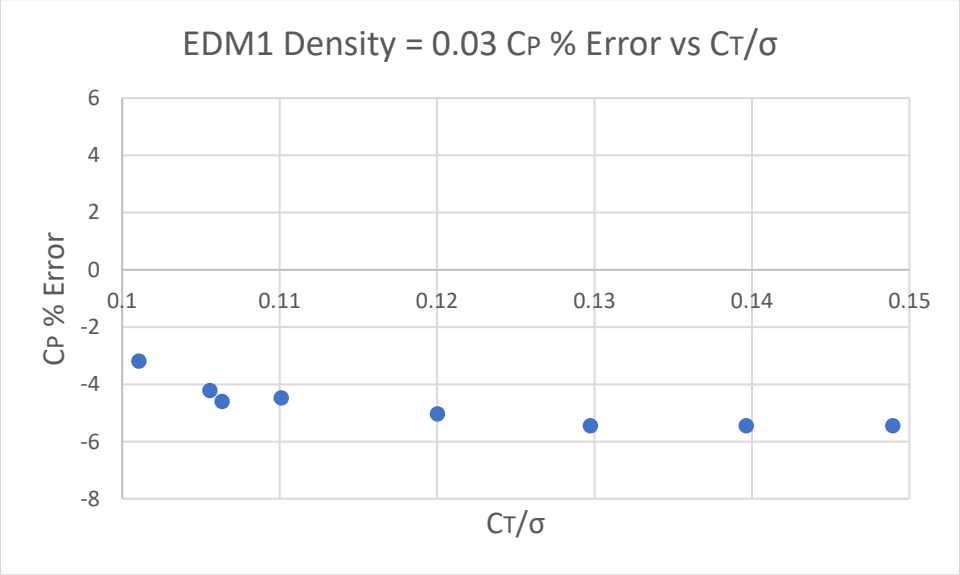

Figure 39: C_P % Error vs C_T/σ for Density = 0.03 EDM1 Results and Final Modified CAMRAD II Results

After completing the modifications to both the values of c_d and the angle of attack for c_l and c_m, the C81 tables were plotted to check for any sharp changes or other unrealistic behavior. These plots are provided in Figure 40. Similar to the first modifications, c_l and c_m vs angle of attack plots are simply stretched about the angle of attack axis. The c_d plot changes by exhibiting a more gradual increase in c_d as angle of attack becomes increasingly negative below zero angle of attack while positive values of angle of attack exhibit a more rapid increase in c_d. These plot changes are expected based on the modification used and do not exhibit any sharp changes or unrealistic values.

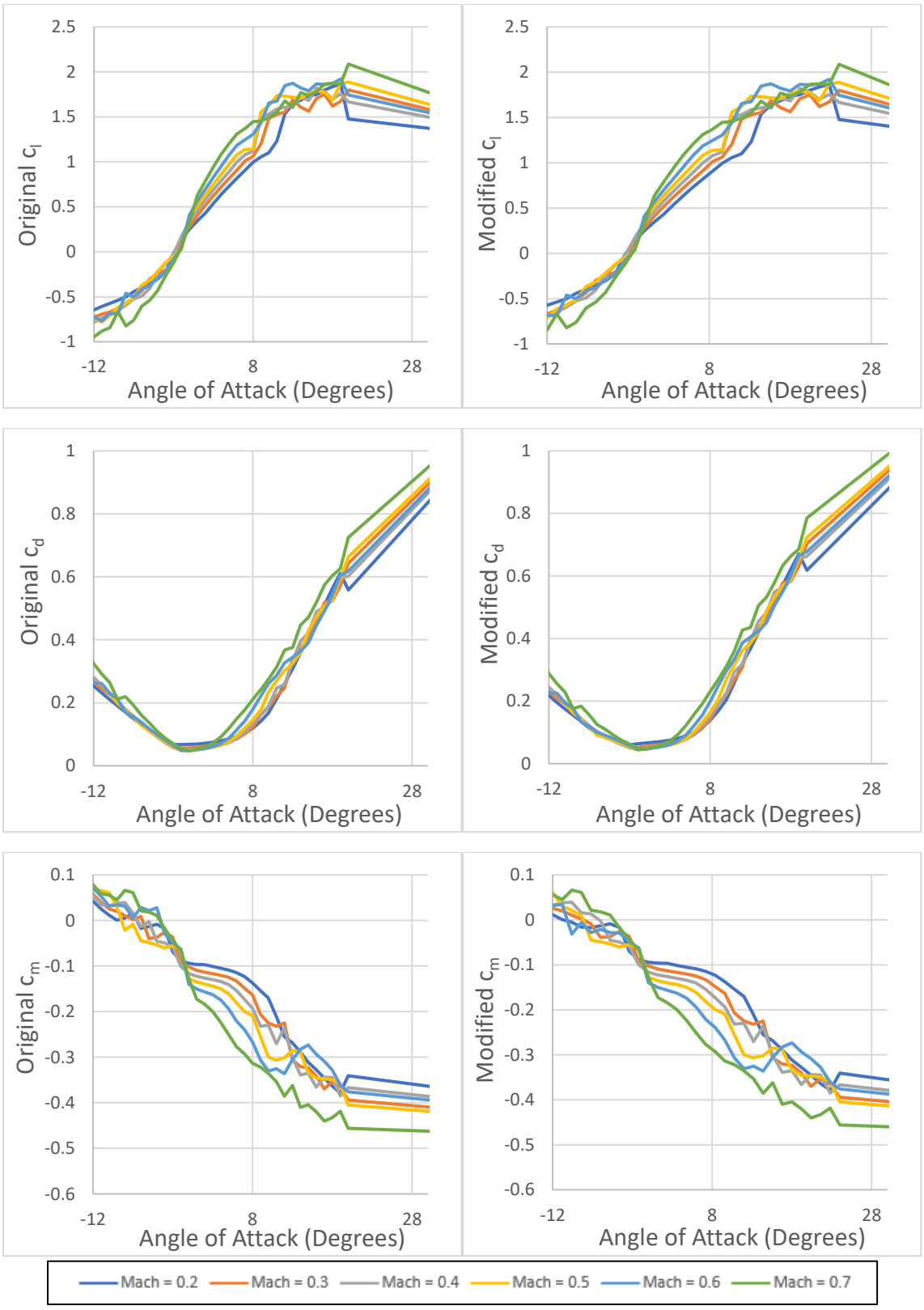

Figure 40: c_l, c_d, and c_m vs α Plots for Original Airfoil Tables (Left) and Final Modified Airfoil Tables (Right) for Radial Station 6 (r/R=0.7620)

While these modifications provided accurate CAMRAD II predictions for EDM1, similar to how angle of attack modification was not consistent for all TRT tests, the EDM1 modifications did not consistently fit the TRT experimental data. Since the EDM1 tests provided a more direct simulation of Ingenuity performance due to the coaxial configuration, the same modifications that were applied to the EDM1 airfoil decks were also applied to the TRT CAMRAD II simulations. The results of those modifications are shown in Figure 41 through Figure 55.

While the overall slopes of the C_T/σ vs collective curves for the modified airfoil decks are closer to the experimental data than the original CAMRAD II data, the curves still overpredict C_T/σ at high collectives. Additionally, at collective values below 10 degrees, the modified airfoil deck results do not significantly differ from the original CAMRAD II results and still underpredict C_T/σ. This slight overprediction at high collective angles and underprediction at low collective angles is consistent for all RPM values.

Unlike the C_T/σ vs collective curves, the FM vs C_T/σ curves exhibited a dependence on RPM. At lower RPM, the CAMRAD II results with the airfoil deck modifications predicted FM values significantly below the experimental values above C_T/σ values of 0.10. As RPM increases, the modified airfoil deck predictions were much closer to the experimental values. The only significant RPM independent observation for the FM vs C_T/σ curves was that at C_T/σ values below 0.10, the FM values predicted by CAMRAD II were almost identical before and after airfoil deck modification. This similarity is expected based on the similar C_T/σ values at low collective for all rotor speeds.

While the FM vs C_T/σ curves were RPM dependent and typically underpredicted, the C_P vs C_T curves for all rotor speeds were closer to the experimental values. For all speeds, the C_P was slightly overpredicted, but only at C_T values above 0.01. For C_T values below 0.01, the airfoil deck modification results align closely with both the original CAMRAD II results and the experimental results.

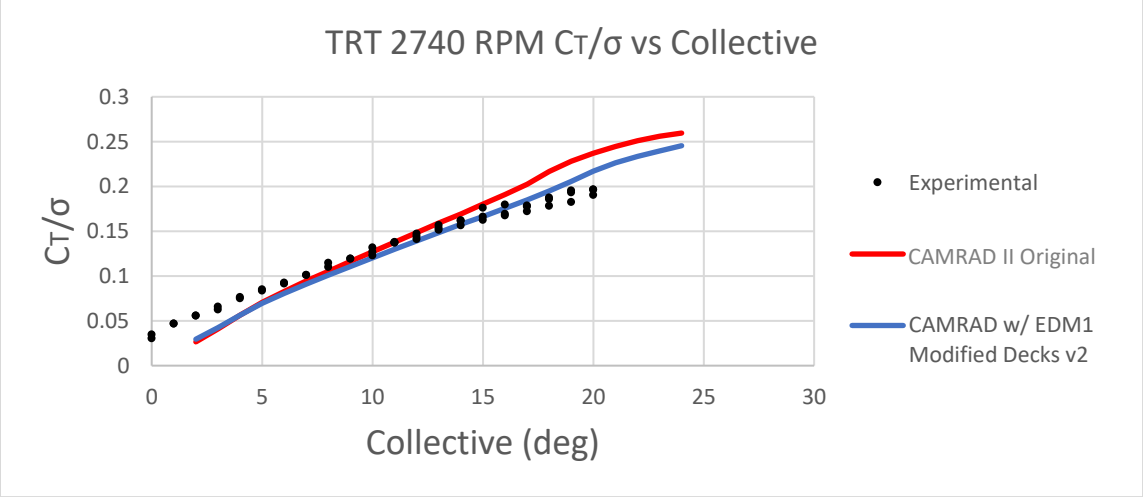

Figure 41: TRT 2740 RPM C_T/σ vs Collective with Final EDM1 Modifications

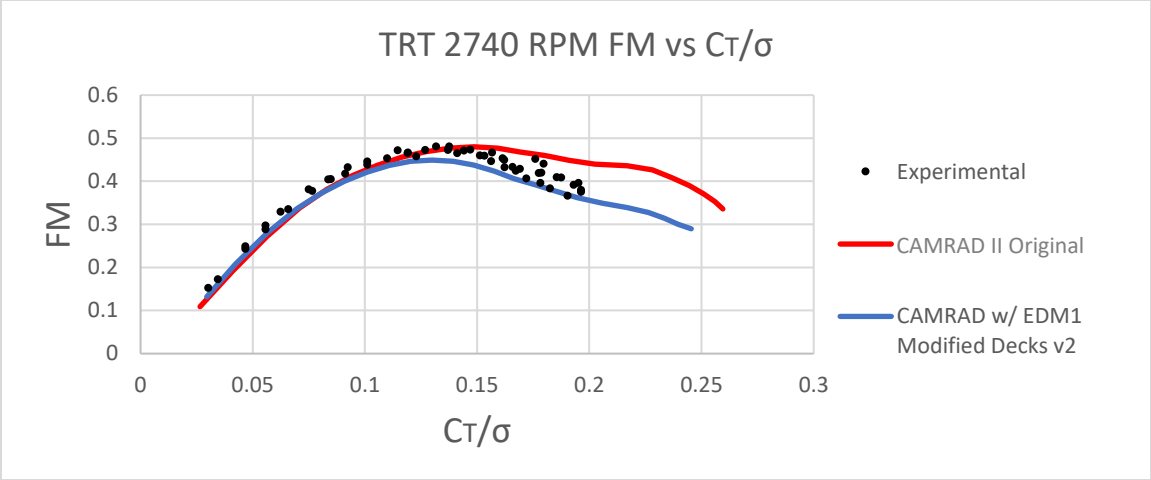

Figure 42: TRT 2740 RPM FM vs C_T/σ with Final EDM1 Modifications

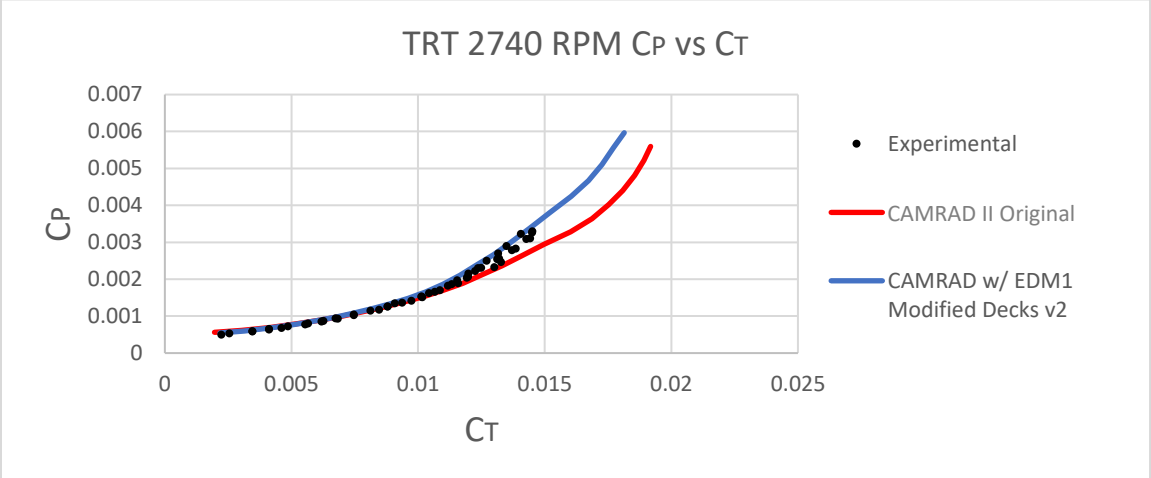

Figure 43: TRT 2740 RPM C_P vs C_T with Final EDM1 Modifications

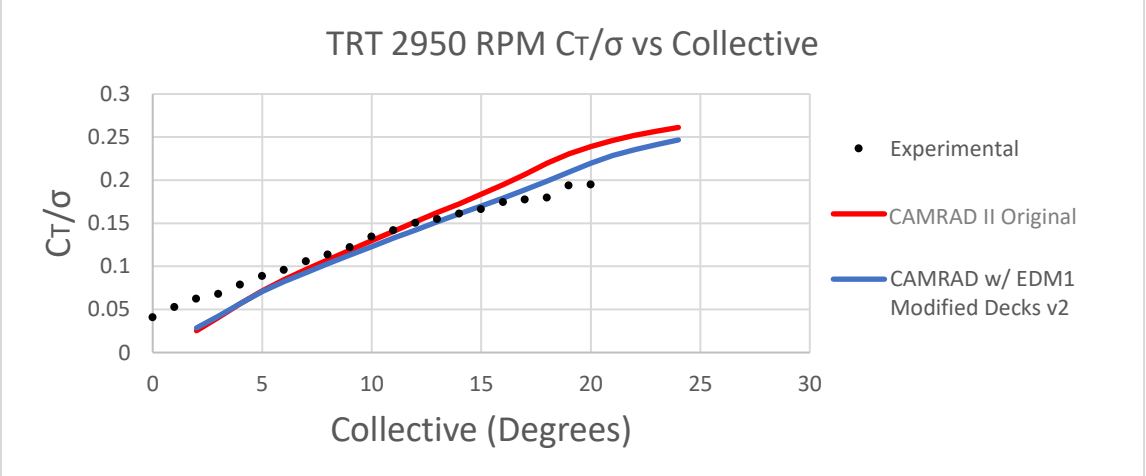

Figure 44: TRT 2950 RPM C_T/σ vs Collective with Final EDM1 Modifications

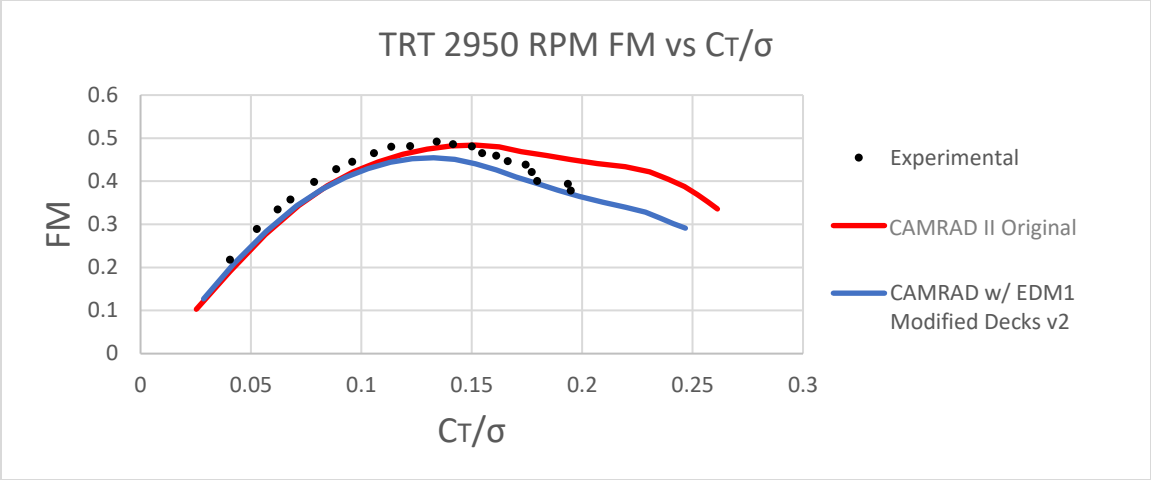

Figure 45: TRT 2950 RPM FM vs C_T/σ with Final EDM1 Modifications

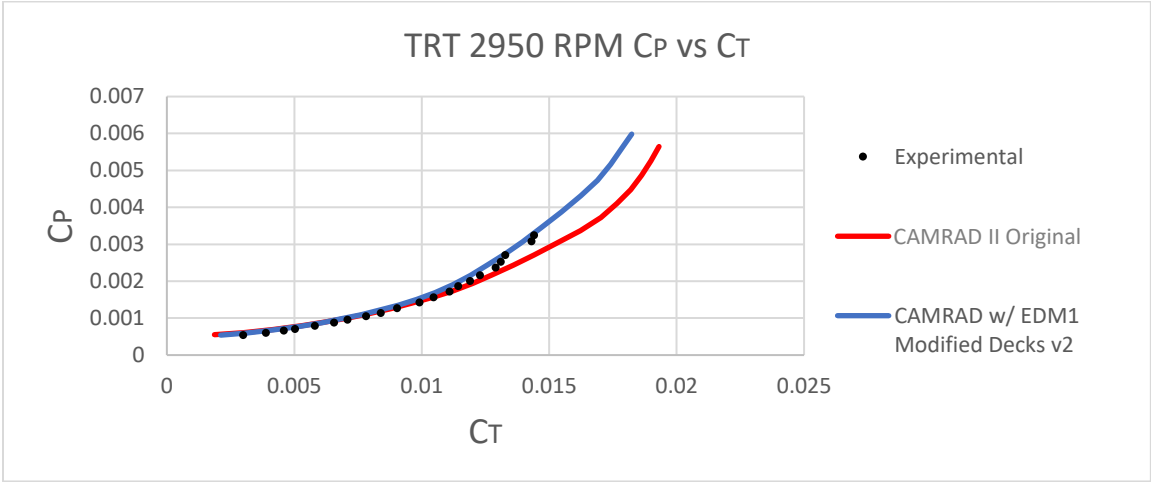

Figure 46: TRT 2950 RPM C_P vs C_T with Final EDM1 Modifications

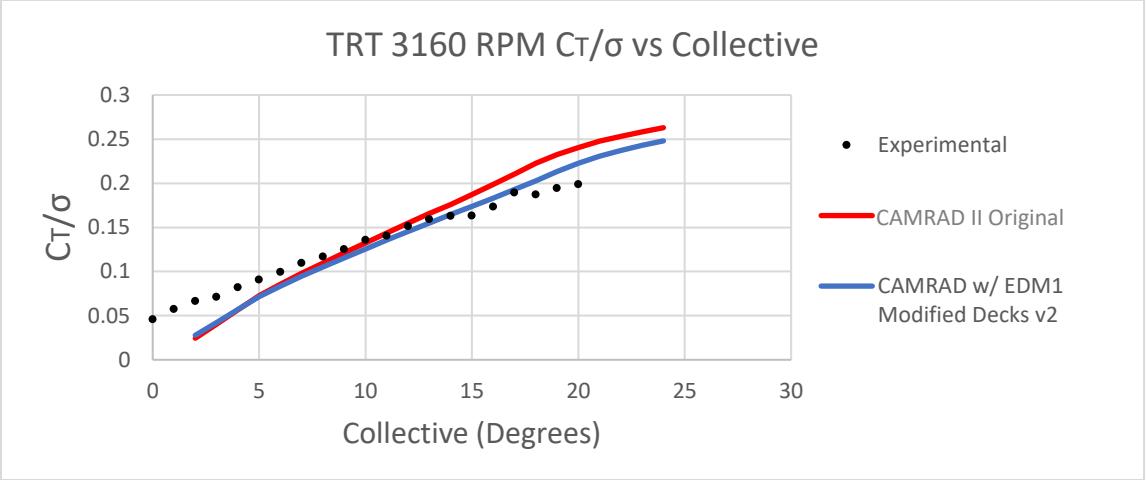

Figure 47: TRT 3160 RPM C_T/σ vs Collective with Final EDM1 Modifications

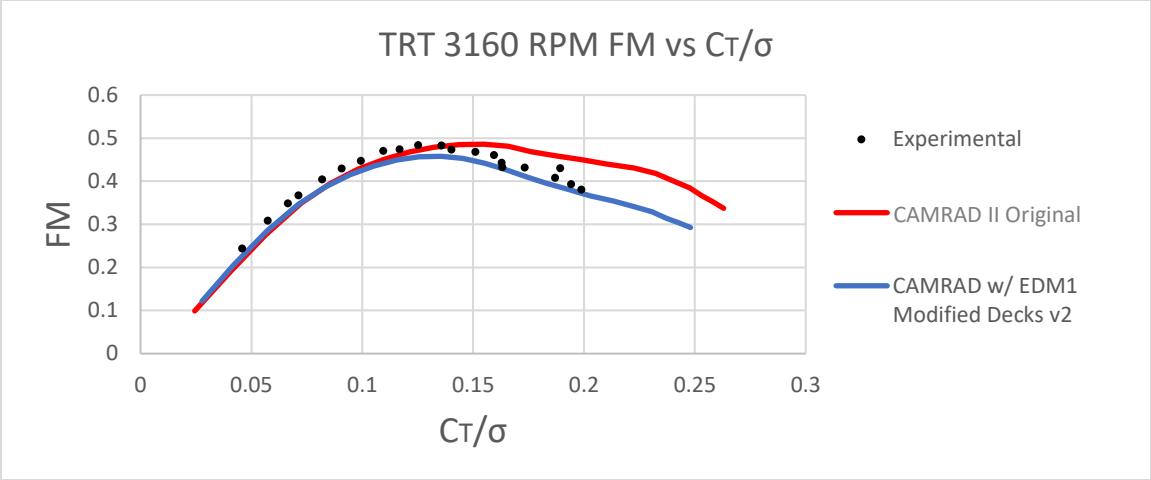

Figure 48: TRT 3160 RPM FM vs C_T/σ with Final EDM1 Modifications

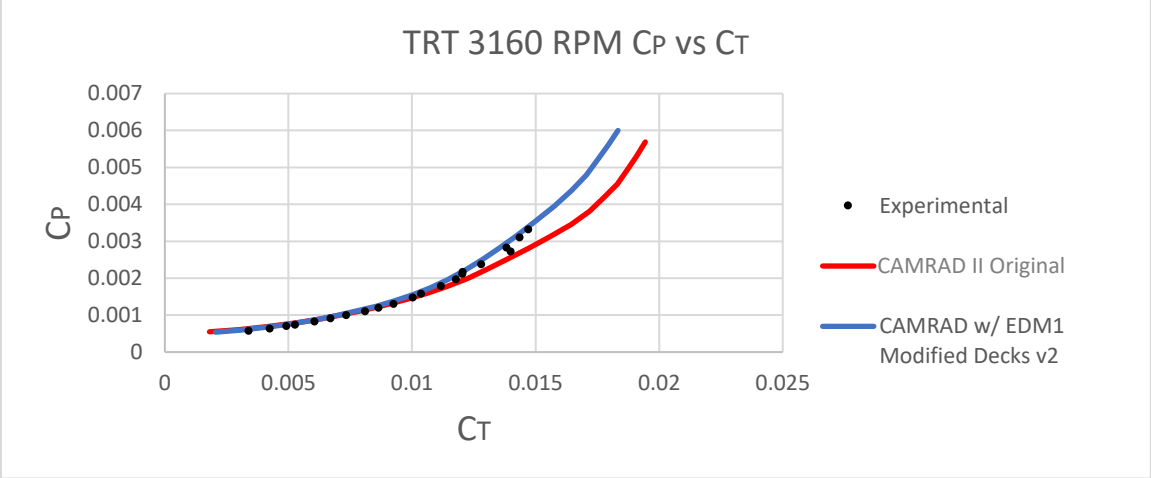

Figure 49: TRT 3160 RPM C_P vs C_T with Final EDM1 Modifications

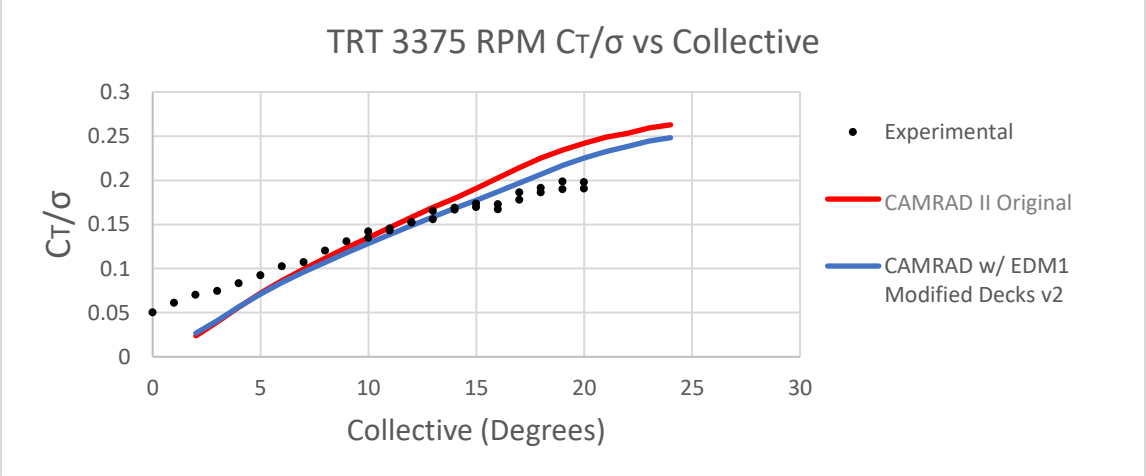

Figure 50: TRT 3375 RPM C_T/σ vs Collective with Final EDM1 Modifications

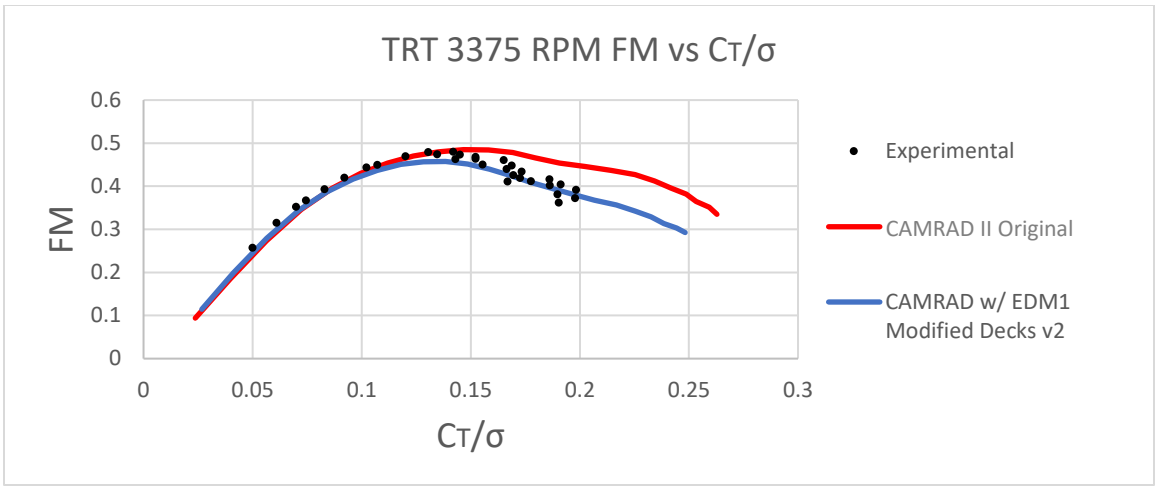

Figure 51: TRT 3375 RPM FM vs C_T/σ with Final EDM1 Modifications

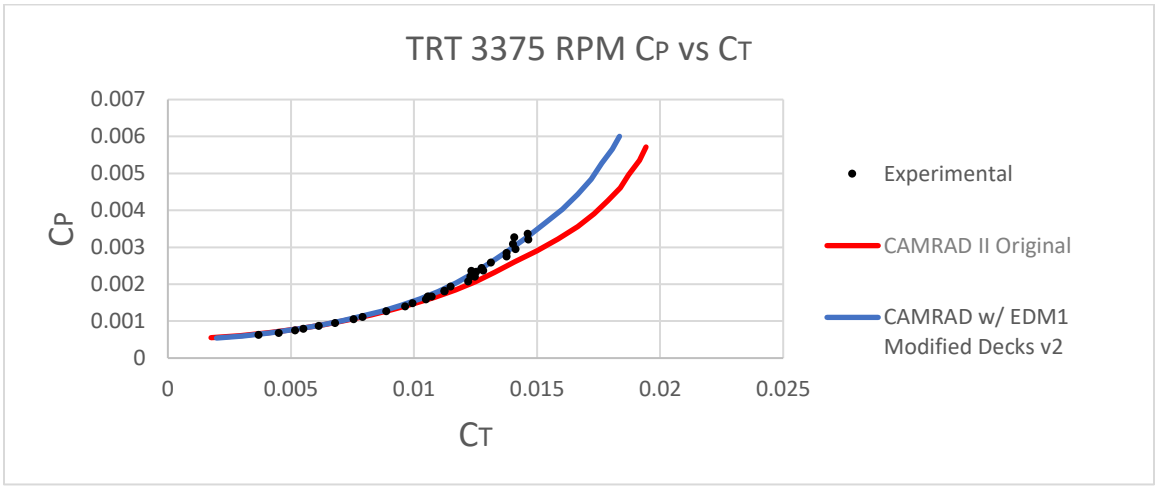

Figure 52: TRT 3375 RPM C_P vs C_T with Final EDM1 Modifications

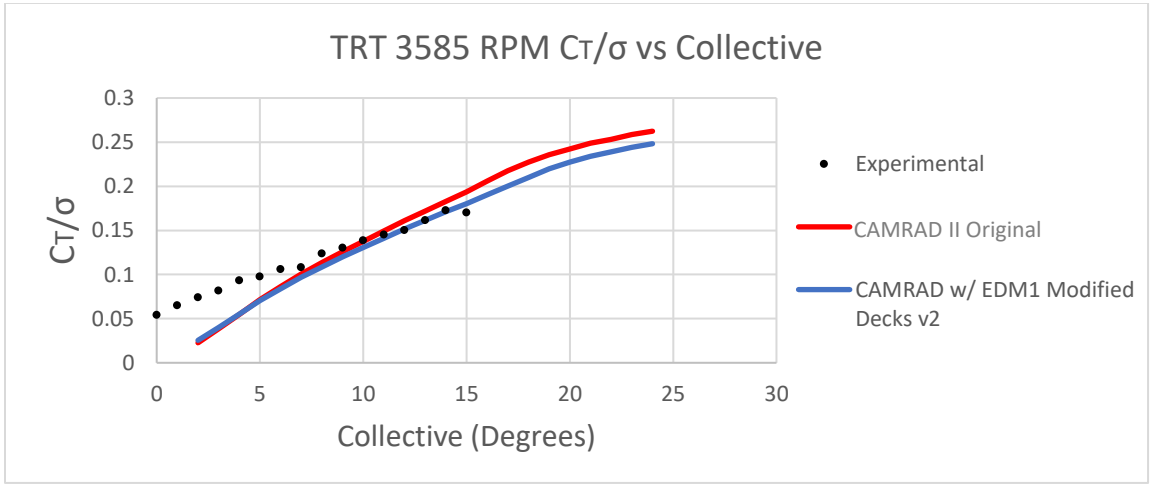

Figure 53: TRT 3585 RPM C_T/σ vs Collective with Final EDM1 Modifications

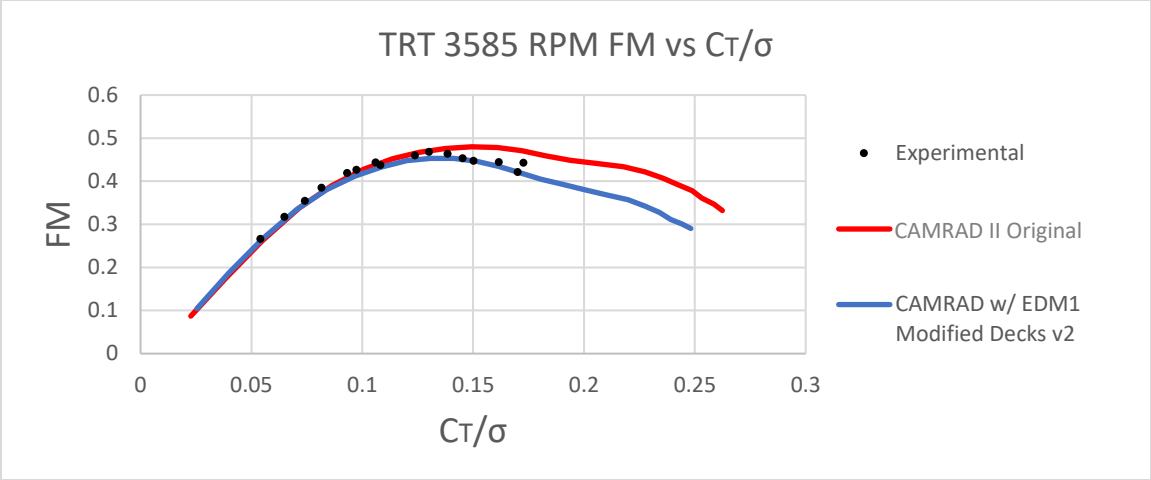

Figure 54: TRT 3585 RPM FM vs C_T/σ with Final EDM1 Modifications

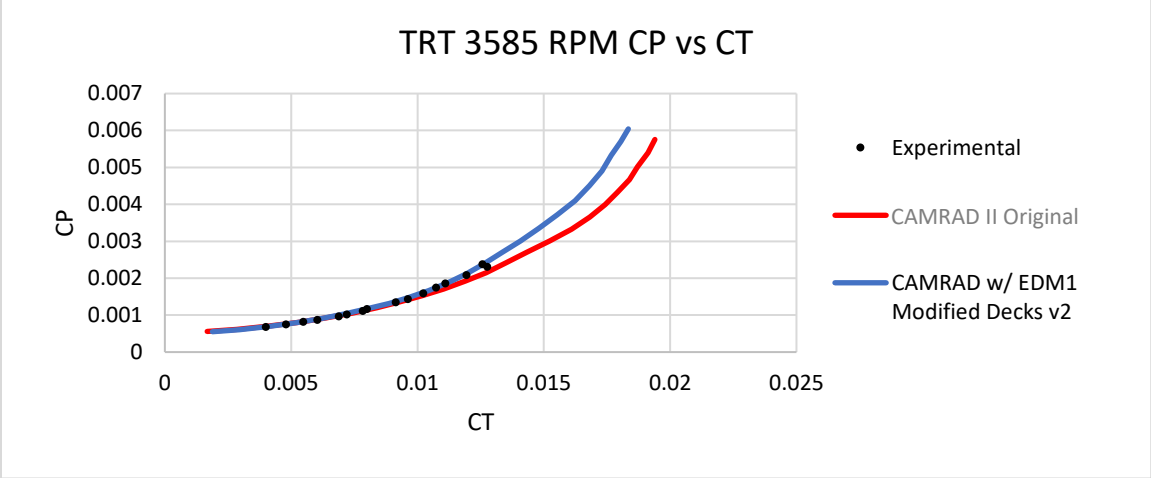

Figure 55: TRT 3585 RPM C_P vs C_T with Final EDM1 Modifications

To better capture and visualize the effects of RPM on FM, the original CAMRAD II results and the modified airfoil deck results were compared to the experimental results at interpolated C_T/σ values of 0.1, 0.125, and 0.15. Those results are shown in Figure 56 through Figure 58, described as the ratio of CAMRAD II predicted FM to experimental FM. While the curves of the two sets of CAMRAD II results have the same shape, the FM values from the EDM1 modified results are consistently lower than both the experimental FM values and the original CAMRAD II results. At higher C_T/σ values the original CAMRAD II results become less conservative and begin overpredicting FM at all tip speeds for C_T/σ = 0.15. In contrast, the EDM1 modified CAMRAD II results follow the same behavior as the original CAMRAD II results but do not become less conservative as a whole.

Additionally, other than a deviation at a tip Mach number of 0.7, both sets of CAMRAD II results yielded higher FM values relative to the experimental values at higher Mach numbers compared to the lower Mach number results. The increase in predicted FM with increased RPM is also more prevalent at higher C_T/σ values. As both the original and modified CAMRAD II results maintain similar shapes independent of C_T/σ value, this RPM dependence indicates that there is still a discrepancy between the experimental results and the CAMRAD II results that is not due to airfoil deck differences.

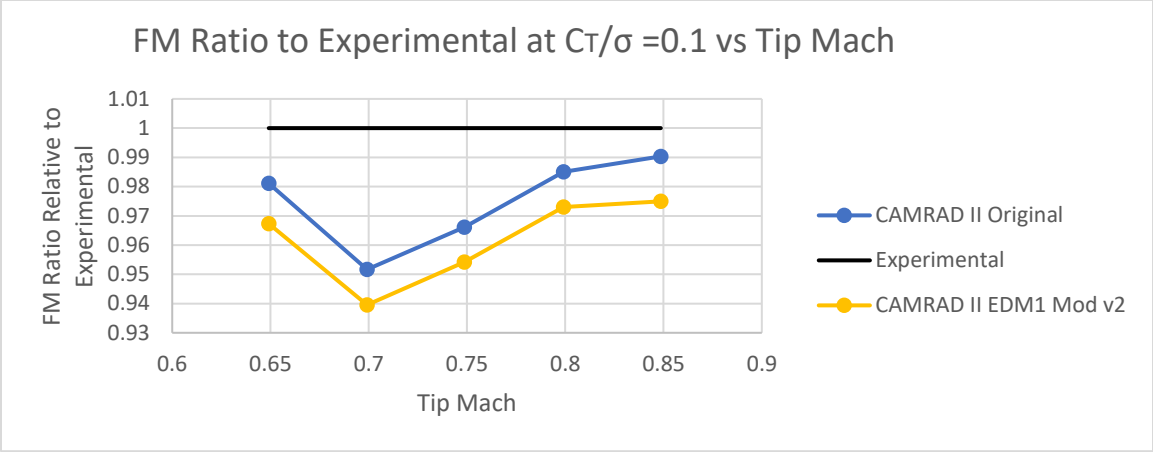

Figure 56: FM Ratio Relative to Experimental Value at C_T/σ=0.10 for Original CAMRAD II and EDM1 Modified CAMRAD II Results at Various Tip Mach Numbers

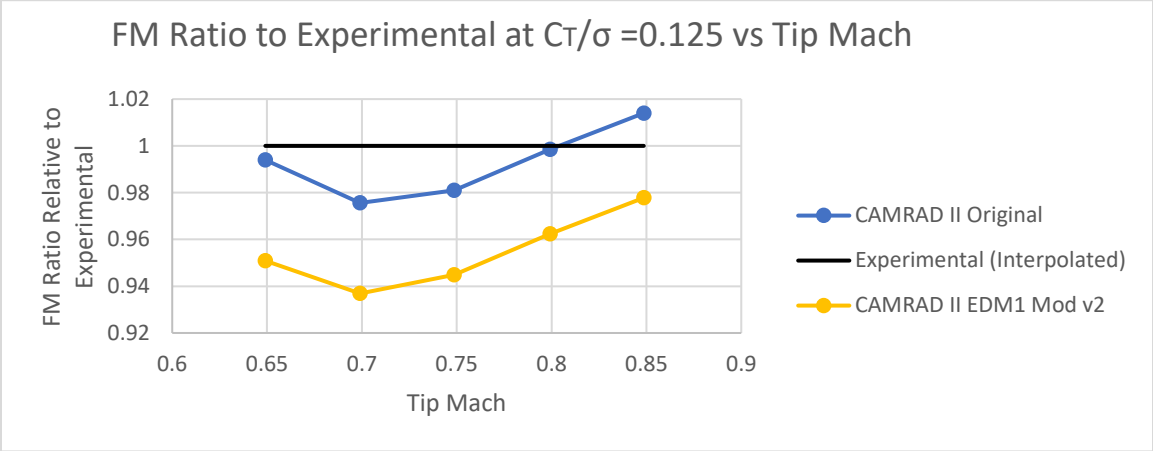

Figure 57: FM Ratio Relative to Experimental Value at C_T/σ=0.125 for Original CAMRAD II and EDM1 Modified CAMRAD II Results at Various Tip Mach Numbers

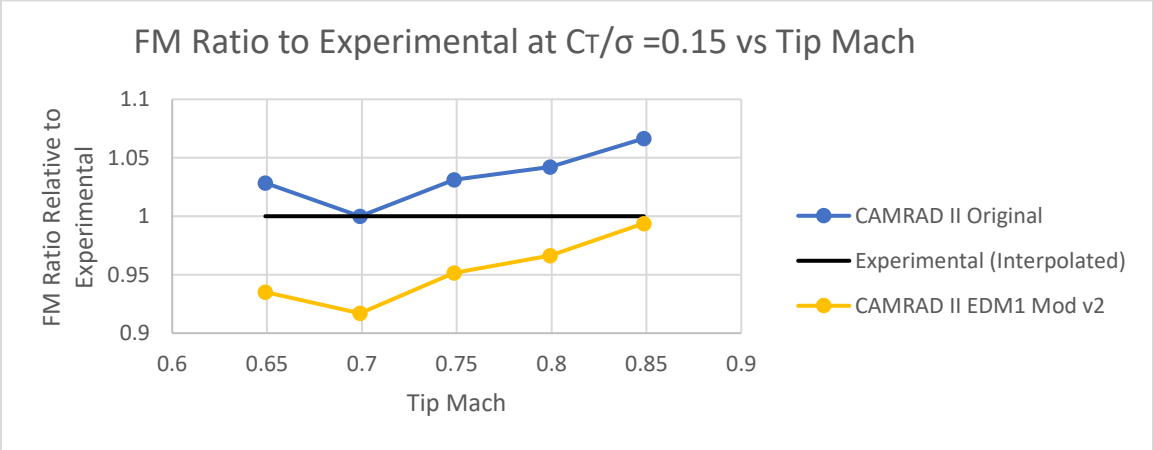

Figure 58: FM Ratio Relative to Experimental Value at C_T/σ=0.15 for Original CAMRAD II and EDM1 Modified CAMRAD II Results at Various Tip Mach Numbers

Conclusion and Recommendations

EDM1 Modifications

For the EDM1 results, the first method of linearly scaling the angle of attack values sufficiently altered the CAMRAD II C_T/σ vs collective results to predict experimental data more accurately. This approach, however, was unable to significantly impact FM vs C_T/σ or C_P vs C_T behavior. The subsequent method of continuing to use the angle of attack modification as well as modification of the c_d values in the airfoil decks did allow for greater accuracy in predicting the experimental results but was unable to produce a single modification that would accurately predict the experiments at all three densities. The final method of using the piecewise function which modified the c_d values while modifying the angle of attack values only for c_l and c_m proved to be the most successful. Using this method, for all three test densities, CAMRAD II was able to accurately predict the experimental data for C_T/σ, FM, and C_P over the full range of collective, C_T/σ, and C_T values respectively.

While the exact physical implications of these modifications are not fully determined, the modified airfoil tables do provide a reference for the correct prediction of coaxial tests of the Ingenuity rotor. As similar methods have been used previously and these modifications provided accurate predictions of experimental data for all three densities, these modifications will be used for future test predictions for Ingenuity blades, and for blades such as those used on SRH, which use the same airfoils [3].

TRT Modifications

The EDM1 modification was less successful for the TRT test results, likely due to differences between coaxial and single rotor aerodynamics and differences between the two test stands (hub and control system), as well as the small influence of RPM (mainly tip Mach number) on dimensionless performance. The EDM1 modification method did provide accurate predictions for some speeds, such as 3375 and 3585 RPM, but a dependence on RPM was evident for FM vs C_T/σ plots and C_P vs C_T plots. However, the C_T/σ vs collective plots were not accurate for any speed, especially at low collective values. These discrepancies indicate that there is some RPM dependent discrepancy between the experimental setup and CAMRAD II model.

References

1) Mier-Hicks, F. et al., “Sample Recovery Helicopter,” 2023 IEEE Aerospace Conference (AERO), 2023

2) Schatzman, N., Chan, A., Gahlot, V., Glazebrook, K., “Data Processing and Analysis of Performance Measurements from Ingenuity Rotors in the Jet Propulsion Laboratory 25-ft Space Simulator,” VFS 6th Decennial Aeromechanics Specialists’ Conference, Santa Clara, CA, February 2024.

3) Grip, H., “EDM1 Helicat Tuning,” Jet Propulsion Laborary Memorandum, 2017.

4) Johnson, W., “Technology Drivers in the Development of CAMRAD II,” American Helicopter Society Aeromechanics Specialist Meeting, San Francisco, California, January 1994.

5) Johnson, W. “Rotorcraft Aerodynamic Models for a Comprehensive Analysis.” American Helicopter Society 54th Annual Forum, Washington, D.C., May 1998.

6) Johnson, W., “Influence of Lift Offset on Rotorcraft Performance,” NASA TP-2009-215404, 2009.

7) Koning, W., Allan, B., Romander, E., Johnson, W., "Comparing 3D and 2D CFD for Mars Helicopter Ingenuity Rotor Performance Prediction," 49th European Rotorcraft Forum, Bückeburg, Germany, September 2023.

8) Nichols, R. H., and Buning, P. G. "User's Manual for OVERFLOW 2.2." Langley Research Center, Hampton, VA, 2008

9) Pulliam, T. H., "High Order Accurate Finite-Difference Methods: As Seen in OVERFLOW." 20th AIAA Computational Fluid Dynamics Conference, AIAA Paper 2011-3851, June 2011. https://doi.org/10.2514/6.2011-3851

10) Tramel, R., Nichols, R., and Buning, P., "Addition of Improved Shock-Capturing Schemes to OVERFLOW 2.1." 19th AIAA Computational Fluid Dynamics, AIAA Paper 2009-3988, June 2009. https://doi.org/10.2514/6.2009-3988

11) Pulliam, T. H. "Time Accuracy and the Use of Implicit Methods." AIAA Computational Fluid Dynamics Conference, AIAA Paper 1993- 3360, July 1993. https://doi.org/10.2514/6.1993-3360

12) Pandya, S., Venkateswaran, S., and Pulliam, T. H. "Implementation of Preconditioned Dual-Time Procedures in OVERFLOW." AIAA 41st Aerospace Sciences Meeting, AIAA Paper 2003-0072, Jan. 2003. https://doi.org/10.2514/6.2003-72

13) Koning, W. J. F., Johnson, W., and Allan, B. G. "Generation of Mars Helicopter Rotor Model for Comprehensive Analyses" American Helicopter Society Technical Conference on Aeromechanics Designs for Transformative Vertical Flight, San Francisco, CA, January 2018.

14) Koning, W. J. F., Johnson, W., and Grip, H. F., "Improved Mars Helicopter Aerodynamic Rotor Model for Comprehensive Analyses," *AIAA Journal*, Vol. 57, No. 9, September 2019. https://doi.org/10.2514/1.J058045

15) Koning, W. J. F., Romander, E. A., Cummings, H. V., Perez Perez, B. N., and Buning, P. G. "On Improved Understanding of Airfoil Performance Evaluation Methods at Low Reynolds Numbers." *Journal of Aircraft*, Vol. 60, No. 3, May 2023. https://doi.org/10.2514/1.C037023

16) Chan, W. M., Rogers, S. E., Nash, S. M., Buning, P. G., Meakin, R. L., Boger, D. A., and Pandya, S. "Chimera Grid Tools User's Manual, Version 2.0." NASA Ames Research Center, 2007.

17) Rumsey, C. L., Slotnick, J. P., and Sclafani, A. J. "Overview and Summary of the Third AIAA High Lift Prediction Workshop." AIAA Aerospace Sciences Meeting, AIAA Paper 2018-1258, January 2018. https://doi.org/10.2514/6.2018-1258